Study of Tensile and Fatigue Behavior of a Multiphase Medium Cabon Microalloyed Steel

By

Vijay Kaushik

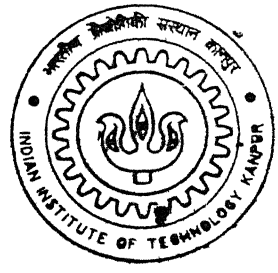

DEPARTMENT OF MATERIALS AND METALLURGICAL ENGINEERING

Indian Institute of Technology Kanpur

FEBRUARY, 2002

Study of Tensile and Fatigue Behavior of a Multiphase Medium Carbon Microalloyed Steel

A Thesis
Submitted by

Vijay Kaushik

For the award of the degree of

Master of Technology

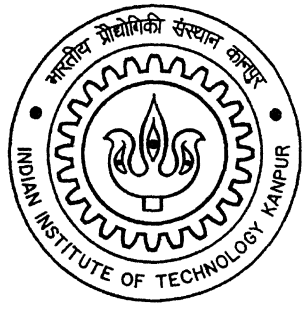

Department of Materials and Metallurgical Engineering
Indian Institute of Technology
Kanpur
February 2002

CERTIFICATE

This is to certify that the thesis entitled "**Study of Tensile and Fatigue Behavior of a Multiphase Medium Carbon Microalloyed Steel**" submitted by Mr. Vijay Kaushik (Roll No. 9910620) to the Indian Institute of Technology, Kanpur for award of Master of Technology is a bona fide record of research work carried out under my supervision. The content of this, in full or in parts, have not been submitted to any other institute or university for the award of any degree or diploma.

Prof. S. Bhargava

Research Guide

Department of Materials and Metallurgical Engineering
Indian Institute of Technology
Kanpur-208016, India.

Kanpur

Date:

ACKNOWLEDGEMENTS

I would like to express my deep sense of gratitude and sincere thanks to **Prof. K.A. Padmanabhan** and **Prof. S. Bhargava,** my research guides for providing me an opportunity to initiate myself in the very interesting area of fatigue of steels. I would also like to thank them for helpful guidance and constant encouragement despite their extremely busy schedule.

I also wish to express my profound thanks to **Dr. M. Sunderaman, Dr. J. K. Chakravartty** and **Dr. S. Banerjee,** senior scientists BARC, for their guidance and help and for allowing me to continue part of the project at BARC Mumbai.

I express my sincere thanks to **Prof. S. Sangal** for his keen interest in my progress, for his constant encouragement and support.

I am thankful to **Dr. Gouthama** for his guidance, valuable suggestions and for help in TEM analysis,

I am very highly indebted to **Mr. B.K.Jain**, lab in charge material testing lab, **Mr. C. Gupta, Mr. J. S. Dubey**, scientists BARC, for their help in carrying out fatigue experiments.

I wish to thanks **Dr, M.N. Mungole** for his help in preparing the metallographic samples and developing negatives.

I am grateful to **Mr. Singh** for his help in carrying out EPMA and fractography.

I have grate pleasure in thanking **Mr. S. Sankaran** for his help, support, suggestions, technical discussions and companying me for tea despite his hectic schedule.

I also wish to thank **Mr.V. Srivastava, Ms. G. Khanna** for their help and useful suggestions.

Lastly, I would like to thank all the faculty members, staff and students of the department for their support and help.

ABSTRACT

Medium carbon microalloyed continuously cooled steels have recently been used as the replacement of quenched and tempered steels for several automotive applications. A constant search for the improvement in their properties is still on. The present investigation was undertaken to obtain a muli-phase microstructure in the medium carbon microalloyed 38MnSiVS5 steel by a special thermomechanical working involving a two step cooling procedure. Thermomechanical treatment involving forging at a finishing temperature of 900-850°C followed by the two-step cooling with (a) air cooling upto 700°C - 680°C after forging and (b) quenching in water immediately after air cooling results in a multi-phase microstructure consisting of bainite/martensite and isolated islands of ferrite phases. On subsequent annealing, this structure gives rise to tempered bainite/martensite. In addition, an increase in ferrite fraction is observed after annealing. An appreciable improvement in strength and ductility is also observed on increasing the annealing time from 1 hour to 2 hours at different annealing temperatures. It is found that the best combination of strength and ductility is obtained on annealing at 450°C for 2 hours. Low cycle fatigue properties are investigated for two conditions (annealed at 450°C and 550°C for 2 hours). Though softening until fracture is observed in both the conditions for all strain levels, the cyclic yield strengths were found to be above 675 MPa. In both the condition, interface between second phase particle and matrix gives rise to the nucleation of microvoids and the crack propagates predominantly by the microvoid growth and their coalescence. The examination of the tested samples under TEM showed that the cyclic loading results in the dislocation cell formation and fragmentation of cementite.

TABLE OF CONTENTS

LIST OF TABLES

LIST OF FIGURES

Chapter 1
INTRODUCTION

In the last decade of 20^{th} century emphases was given on reducing the weight and improving the strength of automotive components to achieve greater passenger safety, driving comfort and to meet the strict environmental regulations. New material and processing routes were developed to fulfill the objective of higher strength and low processing cost. The application of air cooled medium cooled microalloyed steels as a replacement for quench and tempered low alloy steels is now 25 years old. The principal motivation behind the development of these steels is to improve the competitive position of steel forging by a reduction in the cost of the worth component whilst preserving acceptable properties and in-service performance. However there are limitations in the mechanical properties achievable by this processing route if compared with the quenched and tempered process. Two stage cooling, following forging, plus annealing immerged as a promising alternative to continues cooling. This new post forging treatment results in a significant improvement of mechanical properties. High strength and low alloying reduces both cost and the weight of the component.

One of the important life-limiting event for automobile component is fatigue. Most engineering components made of microalloyed steels experience cyclic loading in service, and the cyclic response is significantly different from their monotonic behavior. The effect of various mechanical, microstructural and environmental factors on cyclic deformation as well as crack initiation and growth in a vast spectrum of engineering materials have been the topic of considerable research in the past decades. Strain

controlled cyclic properties of two stage cooled 38MnSiVS5 were investigated in the present work.

1.1 Industrial significance

Cyclic fatigue involves the microstructural damage and failure of material under cyclically varying loads. Structural material, however, are readily designed with composition and microstructures optimizing for fatigue resistance. Metallic alloys are generally designed for strength; yet, if these alloys see engineering service, there structural integrity is often limited by their mechanical performance under cyclic loads. In fact, it is generally considered that over 80 present of all service failures can be traced to mechanical fatigue, whether in association with cyclic plasticity, sliding or physical contact, environmental damage, or elevated temperature. It is always not possible to replicate the actual service condition in laboratory testing, hence any simulation is, of course, a compromise of what is difficult to quantify. Engineering components generally undergo a certain degree of structural constraint and localized plastic flow, particularly at locations of stress concentration, so better approximation can be achieved by strain life approach to fatigue.

Fracture mechanics principles have been very successfully applied to characterization of material fatigue behavior. The fatigue crack growth rate curve, in which crack growth rate is presented as a function of stress intensity range is now commonly used both as a comparative measure of fatigue performance and as a part of engineering standard and design codes.

Chapter 2

LITERATURE REVIEW

2.1 Introduction to High Strength Low Alloy Steels.

High strength low alloy steel (HSLA) comprise a specific group of steel with chemical composition specially developed to import higher mechanical properties values, and, in certain of these steels, materially greater resistance to atmospheric corrosion than is obtainable from conventional carbon steel. HSLA steel is generally produced with emphasis on mechanical properties requirements rather than to chemical composition limits. It is not considered to be alloy steel, even though the utilization of any intentionally added alloy content would technically qualify it as such. Table (2.1) gives the idea of chronology of trends and developments in HSLA steels. The development of HSLA steel is an interesting example of the interplay of technology and economics.

2.1.1 Classification

HSLA can be divided into six categories

(a) Weathering steels, they have ferritic-pearlite microstructure and gain their increased strength principally through elements in solid solution. Because of there great hardness, abrasion resistance is improved; also, if Cu and P are added to the steel, the resistance to atmospheric corrosion is improved to such a degree that the steel need to be painted.

Table 2.1 development of HSLA steels

Period	Focus	Advances in technology
1939-1960	Discovery	Microalloying elements were used in minor way in plate and in structural shapes to ensure the attainment of minimum yield strength.
1960-1965	Research and experimentation of strengthening mechanism	Development of physical metallurgical basis. Hot-rolled semikilled pr fully killed steels. Emphasis on replacing heat treated steel.
1965-1972	Toughening; experimentation on grain refinement and desulfurization	Hot-rolled sheet, plate, pipeline steels, and structural shapes. Development of controlled rolling.
1972 to present	Secondary propertiesand steel making	Emphasis on brittle and ductile fracture control inpipeline and offshore structures, fatigue, resistance toH_2S corrosion, yield behavior , formability of steel, and development of continues casting technology
1979 to present	Reformation and reconstitution	Change in availability of alloying elements such as molybdenum reawakened alloy developers.Previously inaccessible avenues opened by improvements in steel making. Focus on environment degradation.
1980 to present	Diffusion of technology	Cross-fertilization using development from otherproduct areas.
Future	Maturity; trend to higher strengths	Emphasis on reducing alloying costs and processing steps. Reconstitution of the steel to reflect direct hot-rolling and plate mill water-cooling technology.

.

(b) Microalloyed ferrite–pearlite steels, which contain very small (generally, less than0.01%) addition of strong carbide or carbonitride–forming elements such as niobium, vanadium, and/or titanium for precipitation strengthening, grain refinement and possibly transformation temperature control.

(c) As–rolled pearlatic steel, which may include carbon-manganese steel but which may also have small addition of other alloying elements to enhance strength, toughness, formability, and weldability.

(d) Acicular ferrite, in which the ferrite grain are highly irregular in shape with a high dislocation density, about $10^{10}cm^{-1}$, forms by either a bainitic or massive transformation of austenite to ferrite.

(e) Dual–phase steels, which have a microstructure of islands of martensite or lower bainite in ferrite. A typical dual–phase steel could be an HSLA containing about 1.5%Mn and 0.5%Si, strengthened by an addition of about 0.05%V.

(f) Inclusion shape controlled steels, which provide improved ductility and through - thickness toughness by the small addition of calcium, zirconium, or titanium, or perhaps rare- earth elements so that the shape of the sulfide inclusions are changed from elongated stringers to small, dispersed, almost spherical globules.

(g) Hydrogen- induced cracking resistant steel with low carbon, low sulphur, inclusion shape control, and limited manganese segregation, plus copper contents greater that 0.26%.

In the recent years, the automotive industry has been demanding a continuous weight reduction in order to compensate for the introduction of new constructive components according to higher requirement of passenger safety and driving comfort. Furthermore, new strict environmental regulations leading to the control of exhaust gases and reduction in fuel consumption have focused the interest on decreasing the overall weight of the vehicles. Microalloyed steel, which may provide higher strength with smaller alloying addition and less heat treatment expenses, have developed into an important category of engineering materials suitable for the manufacturing of automotive components. Table 2.2 gives the idea of weight reduction achieved on replacing conventional steels by HSLA steels.

2.1.2. Strengthening Mechanisms

All the pure metal and alloys can be strengthened by cold working, or plastic deformation below the recrystallization temperature. In this case, excessive concentration of dislocations is generated and a complex pattern, or network, of dislocations is produced. The mutual interference makes the motion of dislocation extremely difficult. However, along with the strengthening, the ductility and impact strength of the metal decreases simultaneously. Also, metals strengthened by work hardening cannot be joined by welding without the softening the metal in the weld heat -affected zone. For these

Table 2.2 Typical thickness reduction in converting from mild steel to HSLA steels.

Part	Gauge (mm), Mild steel	HSLA Steel	HSLA Yield Strength, MPa.
Front side rail	2.6	2.2	345
Steering-gear mount	3.5	2.7	345
Engine mount	3.8	3.1	345
Suspension cross member	2.3	1.9	345
Bumper reinforcement	3.8	2.9	414
Torque converter plate	3.1	2.5	345
Diamond bracket	9.5	7.8	414
Brake- strut plate	4.5	3.8	414
U- bracket	5.8	4.8	414
Nerf strip	4.4	3.1	414-552
	Body	**Parts**	
Door	0.8	0.7	345
Deck lid	0.8	0.7	345
Hood	0.8	0.7	345
Door hinge	5.0	3.9	345
Hood hinge	3.6	3.1	345
A-pillar	2.3	2.0	380
Door impact beam	1.7	0.8	1034

reasons, this method of strengthening fined relatively little application in high strength low alloy (HSLA) steels. However, very few HSLA steel are designed to make use of work hardening in forming the parts and subsequent strain aging to impart a large increase in yield strength to the as-shipped material [Fletcher,1979].

(i) Grain Refinement

In annealed metals and alloys, the ease with which dislocation can move through the crystal lattice can be reduce significantly by reducing the free path for continues slip. One way in which this can be done is by decreasing the grain size. In the case of controlled-rolled, precipitation- strengthened HSLA structural steel, grain refinement in extensive, thus, it is a significant factor in increasing the strength of HSLA steel. This strengthening mechanism is unique in that it is the only one that improves impact properties concurrent with strengthening.

(ii) Solid Solution Strengthening

Whenever an alloying element is present in solid solution in metal, it hardens and strengthens the solvent metal. Both substitutional solid–solution element that are either appreciable large or smaller than the matrix atom or interstitial atom can lock the dislocation. Most of the carbon that is present in HSLA steel is present in a form other than a solid solution, and only a few hundredths of a percent of carbon strengthens steel in that way [Fletcher,1979]. In semi-killed steel or silicon- killed steel that do not contain strong nitride- forming elements, the small amount of nitrogen present acts as a solid-solution strengthening agent. However, in aluminum killed steel and steel that contain

small amount of columbium, vanadium, or titanium, nearly all of the nitrogen is present as a nitride or carbonitride precipitate; and it has a different function in strengthening the steel.

(iii) Precipitation Strengthening

Although a dislocation can pass through an array of isolated solute atoms in solid solution in the matrix, it can not do so in the case of second- phase particles. The increase in yield strength is associated with the presence of a dispersed second phase in an alloy, and it depends primarily on the strength, structure, spacing, size, shape and distribution of the precipitate particles, on the degree of misfit or coherency between the particles and the metal matrix, and on the orientation of the particles.

2.1.3 Mechanical Properties of HSLA Steels

Blarasin and Farette (1988) tested five hot forged microalloyed steels covering the typical strengthening range of automotive components. The composition and monotonic properties are given in the Table 2.3, and the fatigue properties are given in the Table 2.4.

Kasper et al. (1997) have studied the effect of forging temperature and post forging treatment on microalloyed steel containing V/TiV and carbon about 0.3wt%. they have reported the yield strength varied from 550 MPa to 850 MPa continuously cooled steel after forging. Ultimate tensile strength varied from 950 MPa to 1250 MPa and 0.2% proof strength from 600MPa to 900 MPa for two- stage cooled plus annealed steel. Improvement in percentage reduction in area is also reported with increasing annealing

temperature. The mechanical properties reported for 27MnSiVS6 and 38MnSiVS6 is shown in the Table 2.5

2.2 Thermomechanical Processing

Controlling the deformation condition which leads to improvement in mechanical properties gain importance during second world war. These techniques are designed to use the metallurgical changes caused by deformation to improve heat treatment effect on the properties of steel. Controlled–rolling, controlled- cooling and direct- quenching are typical examples of thermomechanical processing.

2.2.1 Controlled Rolling

Rolling conditions are controlled in such a way to introduce a high density of nucleation sites for ferrite grains in the austenite matrix during the transformation which causes the refinement of structure after transformation. In the controlled rolling of silicon–manganese steel which do not contain any element retarding the recrystallization of austenite, recryatallized austenite grains are refined by performing several hot deformation in the final stage of rolling at the lowest temperature (950-800°C), the refinement of the ferrite grain is achieved by the transformation from the fine- grained austenite structure. Hot deformation temperature plays the most important role to control the austenite structure.

Addition of niobium raises the recrystallization temperature, hence allows a wider temperature range for hot deformation. Other then austenite grain boundaries, twin boundaries and deformation ban are the ferrite nucleation sites introduced by the

Table 2.3 Standard specifications of microalloyed steel [Rodriguez.1998].

Designation	Composition, Wt.%						Properties			
	C	Si	Mn	P	S	V	Yield Strehgth MPa	Tensile Strength MPa	% Elongation	% Reduction in Area
27MnSiV6	0.25/0.30	0.50/0.80	1.3/ 1.60	≥0.035	0.03/ 0.05	0.08/ 0.13	> 500	800-950	> 14	>30
38MnSiVS5	0.35/0.40	0.50/0.80	1.20/1.50	≥0.035	0.03/ 0.065	0.08/ 0.13	> 550	820-1000	> 12	> 25

Table 2.4. Composition and mechanical properties of some HSLA steels [Farsetti.1988].

Type	Composition, Wt.%						Properties				
	C	Si	Mn	V	Nb	Other	Yield Strehgth MPa	Tensile Strength MPa	Strain hardening exponent, (n).	K MPa	% Reduction in Area
48MnV5 (M1)	0.45	0.28	0.70	0.10	-	Cr,Ni,Cu	485	783	0.189	1350	46
(M2)	0.21	0.46	1.54	0.18	0.030	Cr,Ni,Cu,Mo	590	800	0.130	1250	67
(M3)	0.22	0.40	1.68	0.13	0.026	Cr,Ni,Cu	580	875	0.153	1381	48
(M4)	0.54	0.31	0.96	0.11	0.040	Cr,Ni,Cu,Mo	575	930	0.192	1654	45
(M5)	0.38	0.34	1.48	0.10	0.37	Cr,Ni,Cu,Mo	620	940	0.166	1575	54

Table 2.5. Showing the low cycle fatigue results of some HSLA steels [Farsetti.1988].

Steel	Cyclic Properties							
	Strain hardening exponent (n′)	Strength coefficient (K′) MPa	Yield strength (σ_y'), MPa	Fatigue ductility coefficient (ε_f')	Fatigue ductility exponent (c)	Fatigue strength coeficitnt (σ_f'),MPa	Fatigue strength exponent (b)	E_{cyclic}, MPa
48MnV5 (M1)	0.158	1320	495	0.385	-0.551	1165	-0.089	207.1
(M2)	0.098	1210	660	0.677	-0.675	1170	-0.068	209.0
(M3)	0.098	1195	650	0.363	-0.584	1280	-0.079	206.0
(M4)	0.133	1400	600	1.044	-0.689	1290	-0.081	207.7
(M5)	0.150	1612	635	0.931	-0.686	1388	-0.085	205.9

reduction in the non recrystallization temperature range. Improvement in strength ductile to brittle transition temperature and crack arrestability is observed [Tamura, 1988] on finish rolling into ($\alpha+\gamma$) two phase region. The transformation from heavily deformed γ grain after controlled rolling changes the main structure of the steel into fine nonequiaxed and blocky α dispersed with martensite islands and bainite islands [Terazawa,1972; Tamura,1988] showing no indication of the prior γ grain boundaries.

2.2.2 Accelerated Cooling

This cooling process is characterized by accelerated cooling in a γ–α transformation range just after controlled rolling. The grain refinement is due to the decrease in γ–α transformation temperature with a consequent improvement in both yield strength and toughness.

2.2.3 Recrystallization Controlled Rolling (RCR)

The difference between controlled rolling and RCR is the rolling temperature but the difference between conventional hot rolling (CHR) and RCR is not initial obvious because they both rely on high temperature deformation. These are in fact two major differences between RCR and CHR. First, all of the deformation in RCR is completed in the region of full recryastallization. Second, only certain steels are amenable to the RCR method since a mechanism to inhibit grain coarsening must be present in the steel.

2.3 Introduction to Fatigue

The word fatigue is derived from Latin expression fatigare, which means 'to tire'. Fatigue can be defined as a term, which ' applies to change in properties which can occur in a metallic material due to the repeated application of stresses or strain, although this term applies specially to those changes which leads to cracking or failure'.

Interest in the study of fatigue began to expand with the increasing use of ferrous structures, particularly bridges in railway systems. The first detailed research effort into metal fatigue was initiated in 1842 following the railway accident near Versailles in France [Suresh, 1997].In Germany during the 1850s and 1860s A.Wöhler performed many laboratory fatigue tests under repeated stresses. These experiments were concerned railway axle failure and are considered to be the first systematic investigation of fatigue. Wohler introduced the concept of the S-N diagram and the fatigue limit. He pointed out that for fatigue the range of stress is more important then the maximum stresses [Wöhler. 1967; Fuchs, 1977]. Gerber along with others, investigated the influence of mean stress, and Goodman proposed a simplified theory concerning mean stress.

During the 1930s an important practical advance was achieved by the introduction of short pining in the automobile industry, where fatigue failure of springs and axles has been common. Alment [Alment,1963; Fuchs, 1977] explained the spectacular improvements by compressive stresses produced in surface layer of peened parts. In 1950s, Irwin introduced the stress intensity factor KI, which has been accepted as the basis of linear elastic fracture mechanics (LEFM) and of fatigue crack growth life predictions. In the early 1960s low cycle strain-controlled fatigue behavior become prominent with the Coffin–Manson relationship between plastic strain amplitude and

fatigue life. Paris [Paris, 1963; Fuchs, 1977] in the early 1960s showed that fatigue cracks growth rate da/dN could best be described using the stress intensity factor range ΔK.

2.3.1 Different Approaches to Fatigue

To the necked eye, the progress of fatigue is mysteriously devoid of features until the catastrophic growth of a macrocrack in the final few cycles [metal fatigue damage]. The progression of fatigue damage can be broadly classified into the following stages:

(a) Substructural and microstructural changes which cause nucleation of permanent damage.

(b) The creation of microscopic cracks.

(c) The growth and coalescence of microscopic flaws to form 'dominant' crack, which may eventually leads to catastrophic failure.

(d) Stable propagation of the dominant macrocrack.

(e) Structural instability or complete fracture.

The condition of nucleation of microdefect and the rate of advance of the dominant fatigue crack are strongly influenced by a wide range of mechanical, microstructural and environmental factors.

(i) Total Life Approach

Classical approach to fatigue design involves the characterization of total fatigue life to failure in terms of the cyclic stress range (the S-N curve approach) or the (plastic or total) strain range. In these methods, the total number of stress or strain cycles necessary to cause failure in an uncracked (and normally smooth–surfaced) laboratory

specimens is estimated under controlled amplitude of cyclic stress or strains. The resulting fatigue life incorporates both, the number of fatigue reversals to initiate a dominant crack and to propagate this dominant flaw until catastrophic failure occurs. Under high–cycle, low stress fatigue situations, material deforms primarily elastically; the failure time or the number of cycles to failure under such high–cycle fatigue has traditionally been characterized in terms of the stress range. However, in low–cycle fatigue associated stresses are high enough to cause appreciable plastic deformation prior to failure. Under these circumstances, the fatigue life is characterized in terms of strain range. The low–cycle approach to fatigue design has found particularly widespread use in ground-vehicle industries.

(ii) Defect–Tolerant Approach

Preexisting flaws or crack–like defects with in material reduce or may eliminate the crack initiation portion of the component. Thus, the useful fatigue life is then defined as the number of fatigue cycles or time to propagate the dominant crack from the initial size to some critical dimension. The choice of the critical size for the fatigue crack may be based on the fracture toughness of the material, the limited load for the particular structural parts, the allowable strain or the permissible change in the compliance of the component. Fracture mechanism methodology enhances the understanding of the initiation and propagation of fatigue crack and assists in solving the problem of designing to prevent fatigue failures. In terms of the requirement of linear elastic fracture mechanics, the defect–tolerance method is applicable under condition of small–scale yielding, where the crack tip plastic zone is small compared to the characteristic

dimensions of the cracked component and where predominantly elastic loading condition prevail. This conservative approach to fatigue has widely used in fatigue–critical application where catastrophic failure will result in the loss of human lives; examples include the aerospace and nuclear industries.

2.3.2 Structural Features of Fatigue

On the basis of structural changes during cyclic loading, fatigue process can be divided in following stages:

(a) Crack Initiation

This includes the early development of fatigue damage. The deformation due to cyclic loading take place by slip on the same atomic planes and in the same crystallographic direction as in unidirectional loading [Gough, 1933; Dieter,1988]. But, in fatigue some grains will show slip lines while other grains will give no evidence of slip. Slip lines are generally formed during the first few thousand cycles of stress. Successive cycles produce additional slip bands, and the persistent slip bands are embryonic fatigue crack, since they open into wide cracks on the application of small tensile strains.

(b) Slip–Band Crack Growth

This is also called stage I crack growth; it involves the depending of the initial crack on planes of high shear stress. The stage-I crack propagates initially along the

persistent slip diameter before the crack propagation change to stage-II. The fracture surface of stage I fracture is practically featureless [Dieter,1988].

(c) Crack Growth on Planes of High Tensile Stress

This is also known as stage II crack growth, the well-defined crack growth occurs in direction normal to maximum tensile stress. By marked contrast the fracture surface of stage-II crack propagation frequency shows a pattern of ripples or fatigue fracture striations. Such striation represent local crack–growth increment pre cycle and have been hypothesized to occur via a mechanism of opening and blunting of the crack tip on loading, followed by resharpening of the tip on unloading [Laird, 1962; Ritchie, 1977] several theoretical models for rely on the fact that, where plastic zones are sufficiently large compared to microstructural dimensions, plastic blunting at the crack tip is accommodated by shear on two slip- systems roughly. 45° to the crack plane [Pelloux,1969]. New crack surface can be created during cyclic crack advance either by simultaneous or alternating slip on these two systems. This damage process is the primary intrinsic mechanism promoting crack advance.

(d) Ultimate Ductile Failure

Occurs when the crack reaches sufficient length so that the remaining cross section cannot support the applied load.

2.3.3 Strain Control Approach

Low–cycle fatigue is characterized by the presence of macroscopic cyclic strain as evidenced by a stress hystresis loop. Depending on material strength and ductility, the upper limit of the low-cycle fatigue regime may very from 100 to 100,000 cycles or more. For common ductile structural materials, the low-cycle fatigue regime is generally limited to less than 50000 cycles. The definition applies to axially loaded, smooth specimens, subjected to constant amplitude stress or strain cycling.

(i) Stress–Strain Hysteresis Loop

When a metal is cycled to produce plastic deformation of a predetermined amount in both tension and compression, the resulting cycle stress- strain response will produce a hysteresis loop similar to that Figure 2.1. During the test, the stress amplitude, $\Delta\sigma/2$, or the total strain, $\Delta\varepsilon$, or the plastic strain, $\Delta\varepsilon_p$, is held constant and dependent variable is measured. The tip of the loops represents the stress and strain limits for each cycle, and the area inside the complete loop is the energy associated with the plastic work per cycle. The work dissipated during fatigue failure is always mush larger than required for failure in monotonic tension test [Marrow,1964]

(ii) Cyclic Strain–Stress Curves

The cyclic stress- strain curve characterizes the relationship between the strain amplitude and stress amplitude in this stage, which normally last for most of the fatigue life. It offers a convenient way for comparison with monotonic stress–strain curve. The cyclic stress- strain curve may be obtained by connecting the tip of stable hysteresis

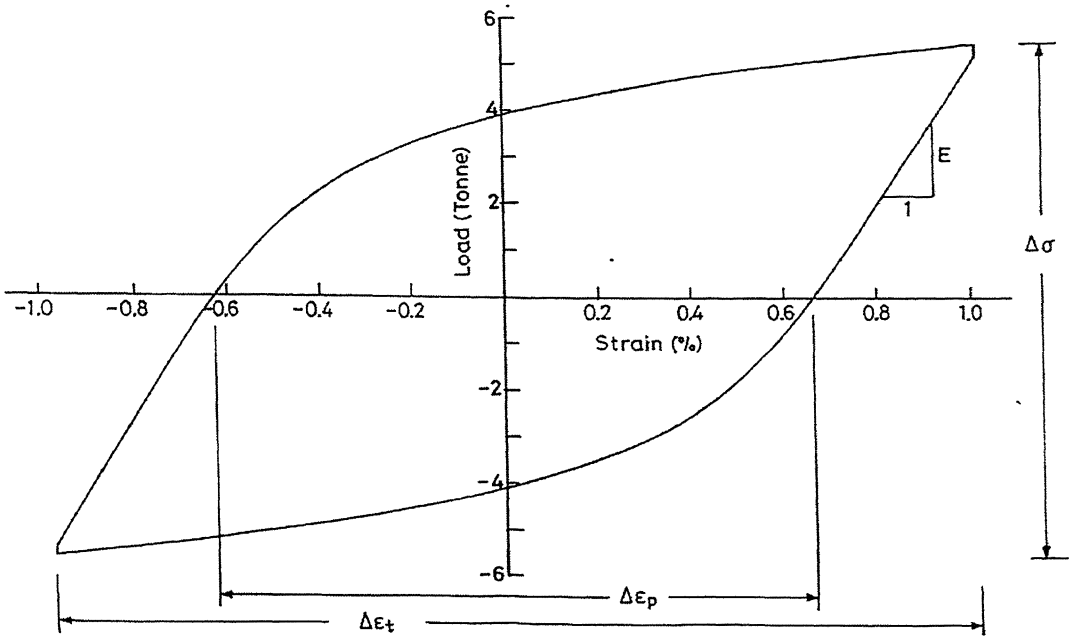

Figure 2.1 A typical hystersis loop.

loops from constant strain amplitude fatigue tests of companion sample at different strain amplitudes. Under condition when no saturation is reached one normally uses either the stress amplitude obtained at half- life, or the maximum stress amplitude for the case of hardening, or the minimum stress amplitude for the case of softening.

(iii) Strain-Life and Stress–Life Curves

Fatigue damage is caused by cyclic plastic strain, and consequently, the fatigue life is related to the plastic- strain amplitude. Coffin and Manson independently proposed a relationship between the plastic- strain amplitude and the cycles to failure:

$$\Delta\varepsilon_p/2 = \varepsilon_f' (2N_f)^c \qquad 2.1$$

Where ε_f' is the fatigue ductility coefficient, $2N_f$ is the number of reversals to failure, and c is the fatigue ductility exponent. The above equation is very similar to the Basquin equation relating the elastic strain to true stress amplitude to the number of load reversals to failure:

$$\Delta\varepsilon_e E /2 = \Delta\sigma/2 = \sigma_f'(2N_f)^b \qquad 2.2$$

Where $\Delta\varepsilon_e/2$ is the elastic strain amplitude, E is the modulus of elasticity, b is the fatigue strength exponent, and σ_f' is the fatigue strength coefficient. The interaction of Basquin and Coffin- Manson plot is normally defined as the transition between high and low cycle fatigue.

2.3.4 Fracture Mechanics Approach

In recent years, fracture mechanics principals have been very successfully applied to the characterization of metal fatigue behavior. The fracture crack growth rate curve, in which the crack growth rate is presented as a function of stress intensity range, is now commonly used both as a comparative measure of fatigue performance and as a part of engineering standards and design code. The classic sigmodial form of the curve produced as asymptotic, 'threshold' value of ΔK, denoted ΔK_{th}, generally defined at or below a da/dN value of 10^{-8} mm/cycle.

One of the goals in fatigue design is to develop reliable method for characterizing the crack growth rate in terms of an appropriate loading parameter which enables a

quantification of the intrinsic resistance of the material to fatigue crack growth for different combinations of applied stresses, specimen geometry and crack geometry. When cyclic stress applied to a component are so small that the zone of plastic deformation ahead of the advancing fatigue crack is a minor perturbation in an otherwise elastic field, linear elastic fracture mechanics solutions provide appropriate continuum description for fatigue fracture.

Paris & Erdogan (1963) suggested that for a cyclic variation of the imposed stress field, the linear elastic fracture mechanics characterization of the rate of fatigue crack growth should be based on the stress intensity factor range,

$$\Delta K = K_{max} - K_{min} \qquad 2.3$$

K_{max} and K_{min} are the maximum and minimum values, respectively, of the stress intensity factor during a fatigue stress cycle. For an edge- cracked fatigue test specimen,

$$K_{max} = Y \sigma_{max} \sqrt{\pi a} \ , \qquad 2.4$$

$$K_{min} = Y \sigma_{min} \sqrt{\pi a} , \qquad 2.5$$

$$\Delta K = Y \Delta\sigma \sqrt{\pi a} , \qquad 2.6$$

$$\Delta\sigma = \sigma_{max} - \sigma_{min} \qquad 2.7$$

where Y is a geometrical factor which depends on the ratio of crack length to the width of the specimen W, and σ_{max} and σ_{min} are the maximum and minimum values, respectively, of the fatigue stress cycle. The fatigue crack growth increment da/dN is related to the stress intensity factor range by the power law relationship

$$da/dN = C(\Delta K)^m, \qquad 2.8$$

where C and m are scaling constants. The exponent m is typically between two and four for ductile metallic alloy. These constants are influenced by such variables as material microstructure, environmental and temperature, and load ratio, R, which is defined as

$$R= \sigma_{min}/ \sigma_{max} = K_{min}/K_{max}, \qquad 2.9$$

Stable fatigue crack growth occurs at stress intensity factor levels, $K_{max}=\Delta K/(1-R)$, that are well below the quasi-static fracture toughness, K_{IC}. In very ductile metallic materials with high fracture toughness, such as low strength steel, the onset of fatigue crack growth can occur at K_{max} values as low as one- hundredth of K_{IC}

2.3.5 Fatigue Crack Propagation in Ductile Metals

The general nature of fatigue–crack growth in metallic material and its description using fracture mechanics can be briefly summarized by the schematic diagram in Figure (2.2) showing the variation in da/dN with the nominal stress-intensity range

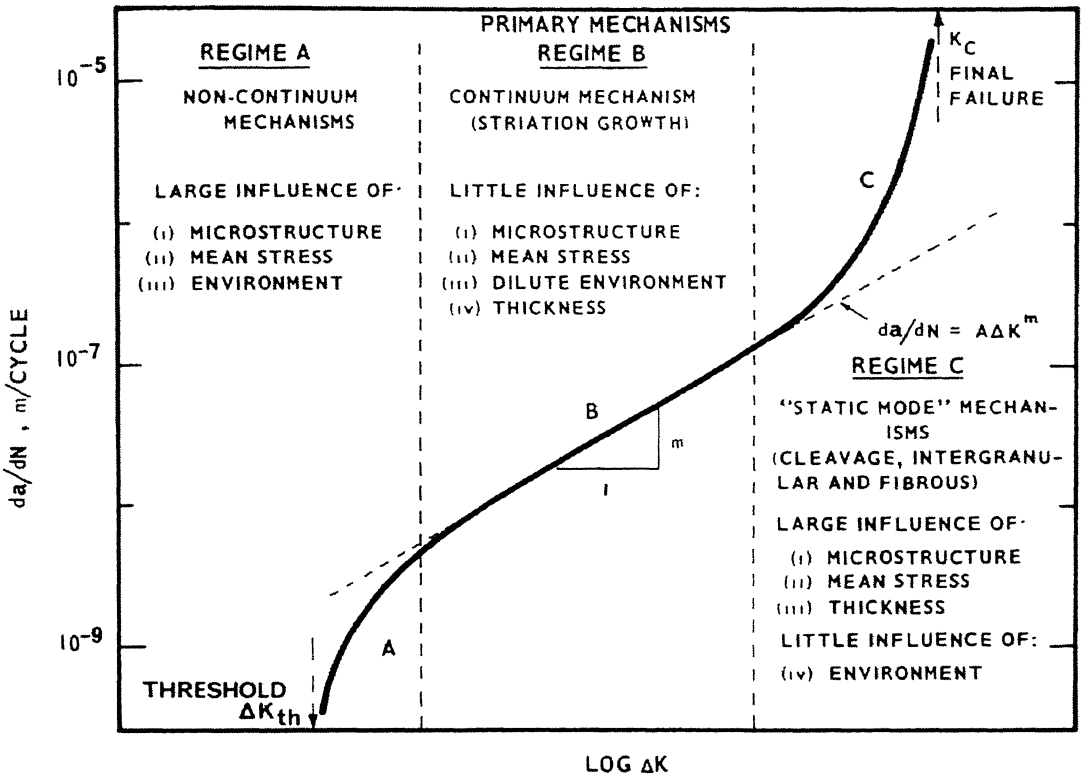

Figure 2.2 Sigmodial variation of fatigue crack growth rate of long cracks as a function of ΔK.

[Ritchie,1977] .In actually, the growth rate depends upon numerous factors other than ΔK, although this is the primary variable in metal fatigue,

$$da/dN = f(\Delta K, K_{max}, \gamma, \text{environment, wave form....}), \qquad 2.10$$

where γ is the frequency.

Specifically results of fatigue- crack growth rate tests for most ductile material display the following characteristics;

(a) Region at low values of ΔK and da/dN (less than $\approx 10^{-9}$ m/cycle) in which fatigue crack appears dormant below the fatigue threshold, ΔK_{th}.

(b) An intermediate range ($\approx 10^{-9}$ to 10^{-6} m/cycle) of power-low behavior described by Paris equation.

(c) An upper region of accelerating crack growth (above $\approx 10^{-6}$ m/cycle) as K_{max} approaches K_c or gross plastic deformation of the specimen, e.g., at the limit load.

The Table 2.6 lists the salient characteristics of the crack advance in the three regimes of stable fatigue fracture [Suresh, 1999].

2.3.6 Factors Affecting K_{th}

(i) Material Strength

Fatigue–crack propagation in metal has been generally found to be largely unaffected by yield strength [Barsom, 1970; Ritchie, 1977]. In fact, for steels raising the strength by nearly an order of magnitude does not change crack- propagation rates over the midrange

Table 2.6 Characteristic of the three regimes of fatigue crack growth.

Regime	A	B	C
Terminology	**Slow growth rate (Near- threshold)**	**Mid-growth rate (Paris regime)**	**High growth rate**
Microscopic failure mode	Stage I, single shear	Stage II, (striation) And duplex slip	Additional static modes
Fracture surface features	Faceted or serrated	Planar, with ripples	Additional cleavage or microvoid coalescence
Crack closer levels	High	Low	_
Microstructural	Large	Small	Large
Load ratio effect	Large	Small	Large
Stress state effect	_	Large	Large
Near- tip plasticity*	$r_c \geq d_g$	$r_c \leq d_g$	$r_c >> d_g$

* r_c and d_g refers to the cyclic plastic zone size and the grain size, respectively.

of growth rate by much more than a factor of two or three. However, at near threshold levels below 10^{-6}mm/cycle, a surprisingly large dependence of material strength has been observed on the value of the threshold ΔK_{th} and on subsequent growth rate [Ritches,1977]. Increase in cyclic strength led to marked increase in near-threshold propagation rates, and a significant reduction in ΔK_{th} Cyclic softening can thus be regarded as extremely beneficial to improving near- threshold fatigue-crack growth resistance in steel [Ritchie, 1977]. The effect of strength on near threshold crack propagation behavior is significantly less at high R values, and not so evident in ferrite-pearlite steel. Coarse- grained precipitation- hardened ferritic microstructures have significantly lower growth rate near ΔK_{th} than higher strength bainitc or martensatic structure [Ritches, 1999].

(ii) Load Ratio

The effect of load ratio on near- threshold fatigue crack propagation rate can be rationalized by crack closer. Condition, such as inert environment or high strength, which hinder the fraction of oxide at low ΔK values result in reduced influence of R- ratio on near threshold fatigue crack growth behavior. For the case of steel expose to inert environment, the dependence of ΔK_{th} on R ratio is less evident than in air this is due to oxide layer formation, which induces crack closer. As the value of ΔK decreases, the influence of load ratio on threshold crack growth rate increases [Liaw, 1982]. The influence on R-ratio on near–threshold fatigue crack propagation can be attributed, at least partially, to some environment interaction. The lack of a load ratio effect at higher growth rate is consistent with this argument, since at such faster propagation rates

pertinent environmental reactions may not be able to keep pace with the crack velocity [Liaw, 1982].

(iii) Effect of Structure and Carbon Content

The microstructure has a strong influence on crack propagation resistance. Ferrite –pearlie steel shows a lower crack propagation rate and a higher threshold stress intensity than martensitic steel. The effect of carbon content on near threshold crack propagation and the threshold stress intensity for pearlite and tempered martensite is not significant [Topper, 1989]. Increase in cold rolling decreases the threshold value and increase crack propagation rate. This can be explained as cold work decreases the crack opening stress level. The threshold stress intensity of an upper bainite is close to that of ferrite-pearlite, while that of a lower bainite is close to that of the quenched and tempered martensitic structure of same steel [Topper, 1989].

Chapter 3

SCOPE OF PRESENT INVESTIGATION

3.1 Material For The present Investigation

Medium carbon microalloyed forging grade steel (38MnSiVS5) was chosen for this investigation. A new post forging treatment, two step cooling, followed by annealing has been applied to achieve multi-phase microstructure.

3.2 Objectives and Scope of the Present Investigation

The following objectives were identified for the present investigation.

i. To establish the two step cooling parameter (quenching temperature) to get the multi-phase microstructure.

ii. To determine the effect of annealing temperature and annealing time on the macrohardness of the microstructure.

iii. To establish annealing time and annealing temperature to achieve optimal monotonic properties.

iv. To determine the low cycle fatigue behavior and study the cyclic softening/hardening behavior at two different annealing temperature.

v. To investigate the strain/life behavior corresponding to different annealing temperatures.

vi. To compute the fatigue life from the cyclic stress-strain and tensile properties and compare then with the experimental findings.

vii. To study the fatigue crack growth rate behavior of steel.

viii. To study the effect of stress-ratio on the fatigue crack growth rate.

ix. To analyze the fracture surfaces resulting from low cycle fatigue and fatigue crack growth rate testing with respect to crack initiation and crack propagation.

x. To study the effect of cyclic loading on the microstructure.

Chapter 4

EXPERIMENTAL PROCEDURE

4.1 As-Received Material

This material, 38MnSiVS5 steel, used in the investigation was produced at Tata Iron and Steel Company, Tata Nagar, India. Its chemical composition is shown in Table 4.1. The material was received in the form of round corner shape billet (125×125mm).

Table 4.1 Chemical composition of 38MnSiVS5 steel

Material	C	Si	Mn	P	S	V	N	Cr	Fe
38MnSiVS6	0.38	0.68	1.5	0.022	0.06	0.11	0.006	0.18	Balance

4.2 Thermomechanical Processing

Forging was carried out at Field Gun Factory, Kanpur. The steel billet was austanized at 1100- 1200°C for 1h in an oil fired furnace which was followed by forging to 80 mm diameter rods; this was again heated in the same temperature range and forged down to 40mm diameter rods. Again the rods were austenized in the same temperature range for 1h, in the final forging the rods were reduced down to 25 mm dia. and the finish forging temperature was 920±10° C. It was followed by continues air cooling to 850±10° C and then quenched in water to room temperature, a simplified flow sheet showing the forging treatment is shown in the Figure 4.1

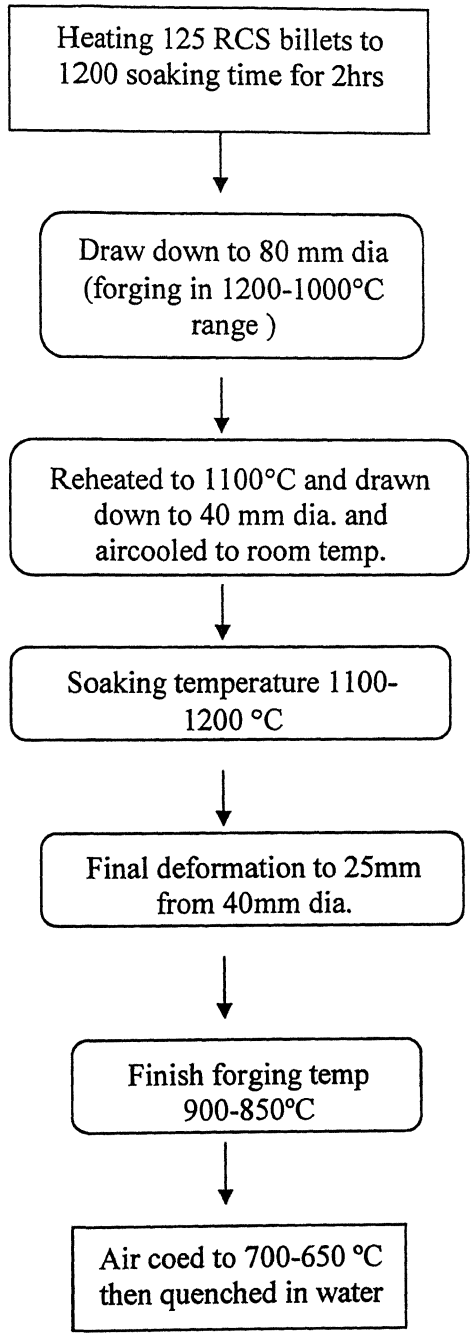

Figure 4.1 Flow sheet showing thermomechanical treatment.

4.3 Annealing Treatment

The forged rods (25mm dia) were annealed in a muffle furnace at various temperatures and for different times, as shown in the Table 4.2.

Table 4.2 Temperature and time of annealing

Temperature	**Time in Hrs.**			
420° C	1	1.5	2	2.5
450° C	1	1.5	2	2.5
480° C	1	1.5	2	2.5
550° C	1	1.5	2	2.5

4.4 Microscopy

For optical microscopy, samples (20mm dia) were taken from the as received, forged (TSC) and annealed rods .These were ground to remove the oxide layer and mechanically polished to mirror finish with emery paper followed by alumina on a polishing wheel. Etching was done using 2% natal (HNO_3 +Alcohol). Approximate prior austenite grain size was measured by line intercept method considering the ferrite grains network as the prior austenite grain boundaries; this is based on the fact that in hypoeutectoid steel ferrite will nucleate on the prior austenite grain boundary. Microstructure was seen under optical, scanning electron microscope (JEOL 5300). Fracture surface was cleaned in acetone before examination under the electron probe microanalyser (JEOL JXA-6300MXA).

(a)

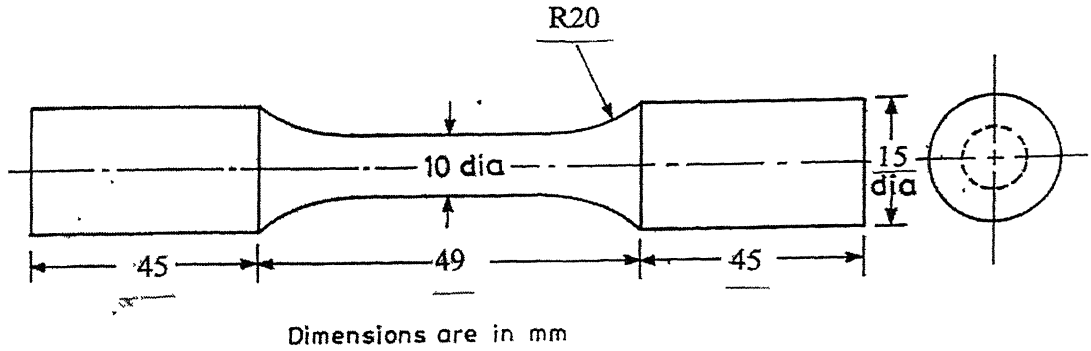

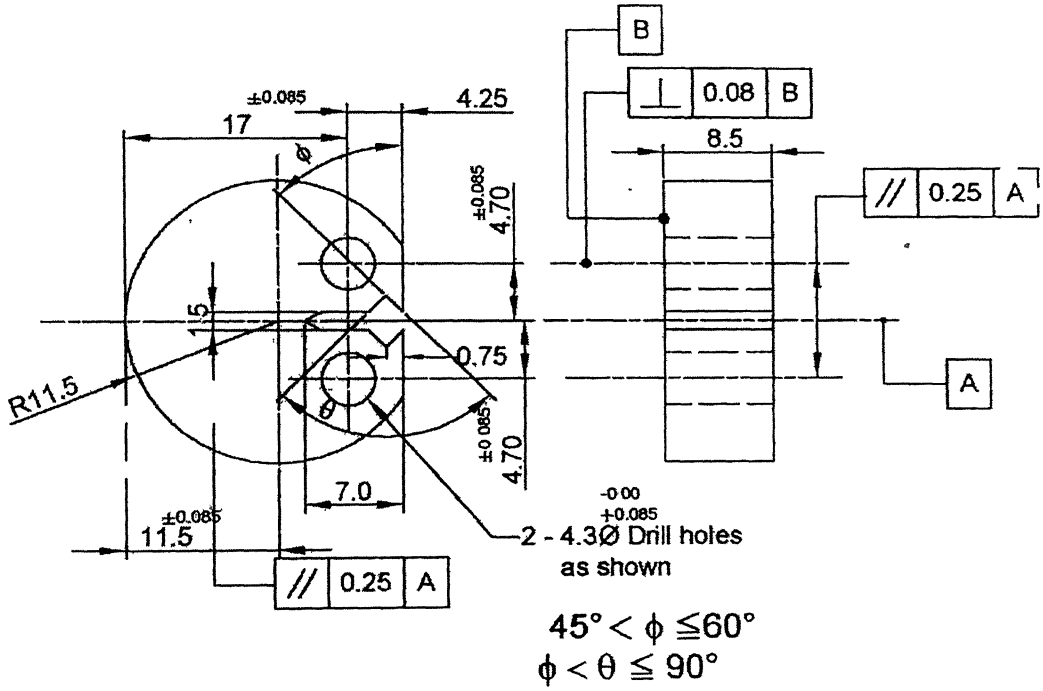

(b)

Figure 4.2 (a) Showing sample drawing used for LCF testing. (b) drawing of sample used for crack growth studies.

4.6 Mechanical Testing

4.6.1 Tensile Test

Room temperature tensile test were done under stroke control at a strain rate of $2\times10^{-3}s^{-1}$ on a 10 T closed loop servo- hydraulic Material Test System (MTS810). A 25 mm extensometer was used to measure the strain. Table 3.3 shows the conditions for which the tensile testing was done.

Table 4.3 Annealed conditions for which tensile properties were investigated

Annealing Time(hours)	**Annealing Temperature**			
	420°C	**450°C**	**480°C**	**550°C**
1	420(A,1)	450(A,1)	480(A,1)	-
2	420(A,2)	450 (A, 2)	480(A,2)	550 (A, 2)

4.6.2 Low Cycle Fatigue Testing

Closed loop servo-hydraulic Materials Test System was used carryout room temperature constant amplitude LCF test under total strain control. The tests were performed using a triangular strain rate of $2\times10^{-3}s^{-1}$. The tests were continued till fracture. A 25mm, extensometer (Model No. 632.11C-20) was used to measure and control strain.

4.6.3 Fatigue Crack Growth Test (FCGR)

The fatigue crack growth rate tests (FCGR) were done according to ASTM standard E 647-88a. Load shedding technique was used to generate various portions of FCGR curves. Servo hydraulic Material Test System (MTS 810) was used to perform the

crack growth tests. The experiment were carried out at f=20 Hz, ambient temperature and atmospheric pressure. Crack length was measured using compliance measurements. The tests were done for two R- ratios 0.1 and 0.4, both with increasing and decreasing ΔK values. The samples were precracked using sinusoidal load cycle at stress intensity of 18–15 $MPam^{1/2}$ and load ratio of 0.1.

4.6.4 Data Acquisition

The data acquisition and analysis was carried out with the help of series 759 software, Matlab, Origin 5.0 and Microsoft Excel.

Chapter 5
RESULTS AND DISCUSSION

5.1 Microstructural Evolution on Thermomechanical Processing followed by Two Step Cooling of 38MnSiVS5 Steel

5.1.1 As Received Microstructure

The chemical composition in wt. % of the medium carbon steel (38MnSiVS5) is given in the Table 4.1 of Chapter 4. The microstructure of as received steel is shown in the Figure 5.1. It is seen that this microstructure consists of ferrite and pearlite which is typical of steels hot deformed followed by air cooling. Measurements made on the ferrite volume fraction and the mean size of ferrite showed that its volume fraction was 30% (standard deviation= 0.052). Similarly, the mean ferrite grain size was found to be ≈18μm.

5.1.2 Microstructure of 38MnSiVS5 after its Thermomechanical Treatment (TMT) followed by Two Step Cooling

It has already been mentioned in Chapter 4 that the as-received rods of 38MnSiVS5 steel were soaked at 1100-1200°C for 60 minutes and were subjected to hot forging at the finishing temperature of 900-850°C. The forged bars were subsequently subjected to the two-stage cooling. The thermomechanical processing followed by two step cooling (TSC) resulted in the pearlite free microstructure in which the volume fraction and size of ferrite grain was drastically reduced as shown in Figure 5.2. The microstructure has well distributed acicular phase which could be bainite/martensit and few isolated islands of free ferrite formed during initial slow cooling from finish forged

temperature. Further, grain size of prior austenite grains, as obtained by the line – intercept method, showed that the thermomechanical processing results in refinement of austenite grains (from 65μm (standard deviation = 1.159) to 34μm (standard deviation = 1.64). It can thus be concluded that the specific area of austenite grain boundaries increases by TMT.

Though no specimen was prepared for the TEM analysis from the steel after its thermomechanical treatment followed by two-stage cooling, the steel is expected to have precipitates of vanadium carbide/carbonitride. In fact, the TEM replica prepared after TMT followed by TSC and annealing (as discussed in the next section of this chapter) showed the presence of such precipitates in the microstructure. Further, if we refer to the CCT diagram of 38MnSiVS5 steel shown in Figure 5.3, as determined by Madariaga et al. (1999), some untransformed austenite is also expected due to the fast cooling in second step. As suggested by Kasper et al. (1997), the ferrite formed during slow first step cooling is expected to be super saturated with carbon. As expected, accelerated cooling in the second step results in bainite/martensite transformation of the remaining austenite.

5.1.3 Microstructure of TSC plus Annealed

As mentioned in Chapter 4 (Table 4.1), the steel after its TMT and TSC was further annealed at the temperatures of 420°C, 450°C, 480°C and 550°C for periods ranging from 1 hour to 2.5 hours. The effect of annealing time and temperature for the temperatures of 450°C and 550°C on the microstructure of steel, as revealed by optical metallography, can be seen in the Figure 5.4. and 5.5. Similarly, the transmission electron

micrograph of the steel after annealing at 450°C for 2 hours is shown in Figure 5.6. It is seen that the annealed microstructure of thermomechanically treated and two-stage cooled steel essentially consists of ferrite, tempered bainite/martensite and precipitates of vanadium carbide/carbonitride. The ferrite which formed at the high temperature and slow cooling rate, nucleated as grain- boundary allotriomorphs and grew into equiaxed grains are clearly observed on annealing the steel at 550°C for 2 hrs, Figure 5.5.

As suggested by Kasper et al. (1997), the decomposition of retained austenite is expected in two-stage cooled 38MnSiVS5 steel during its annealing in the temperature range of 300°C-500°C. This increases the ferrite fraction which can be seen in the annealed microstructure (Figures 5.4& 5.5). However, it is clearly seen that distribution of phases in the microstructure remains acicular on annealing at 450°C for 2 Hrs and the increased ferrite fraction can be seen in the Figure 5.4.

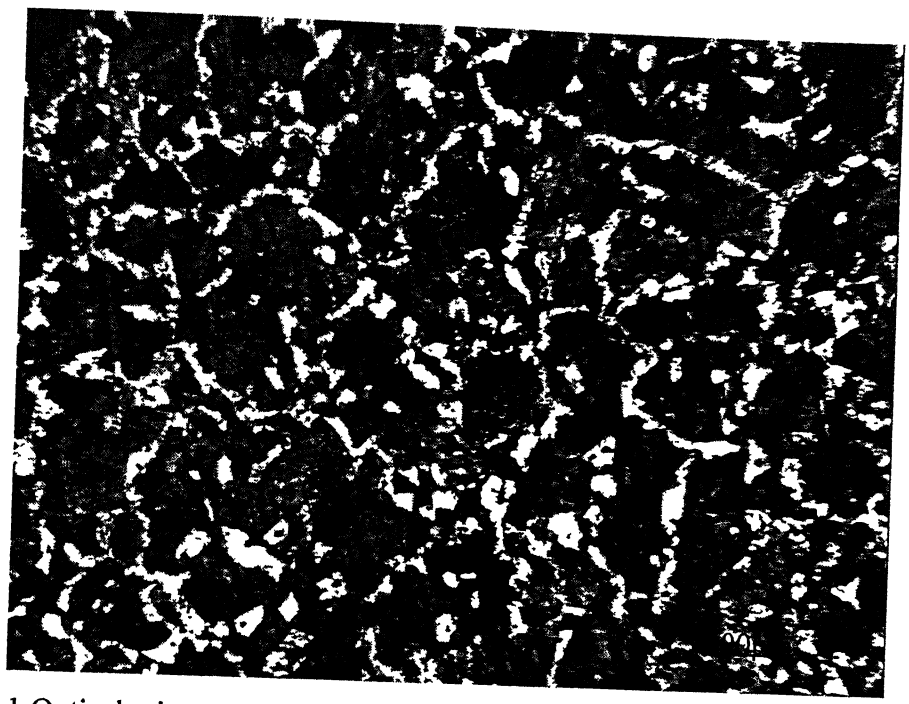

Figure 5.1 Optical micrograph of as received steel.

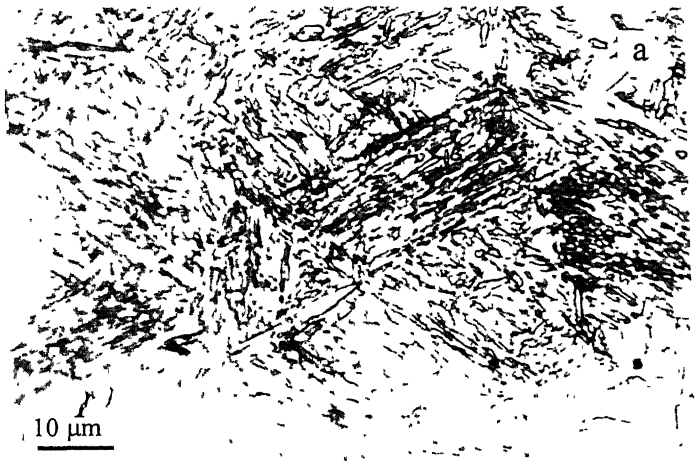
a
10 µm


b
2µm

Figure 5.2 Micrographs showing microstructure after TSC (a) optical micrograph (b) and (c) SEM micrographs.

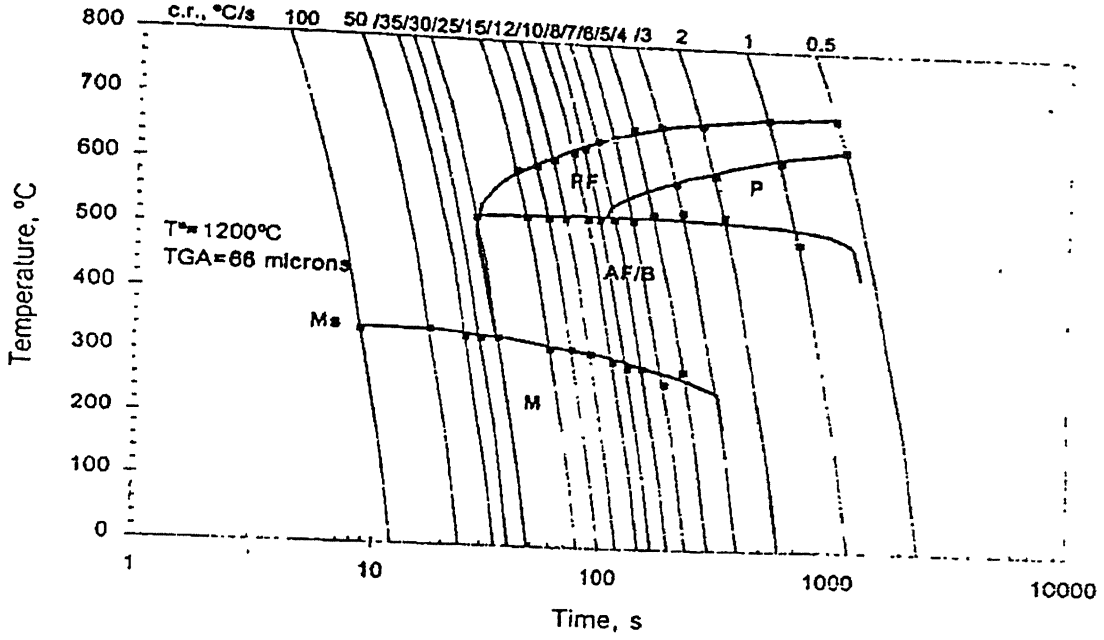

Figure 5.3 Continues cooling transformation diagram for 38MnSiVS5 steel [Madariaga, 1999]

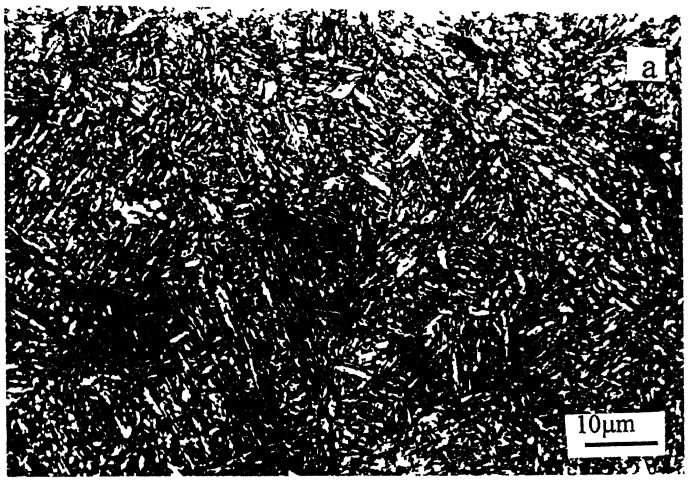

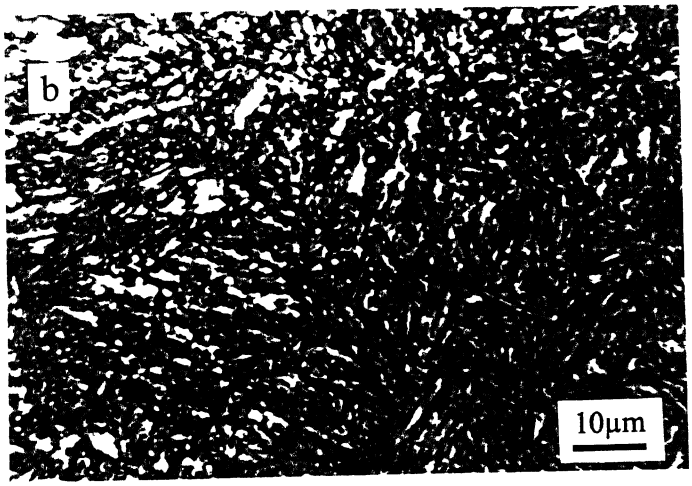

Figure 5.4 Optical micrograph showing microstructures of steel (a) annealed at 450°C for 1.5 hours (b) annealed at 450°C for 2 hours.

Figure 5.5 Optical micrograph showing microstructures of steel (a) annealed at 550°C for 1.5 hours (b) annealed at 550°C for 2 hours

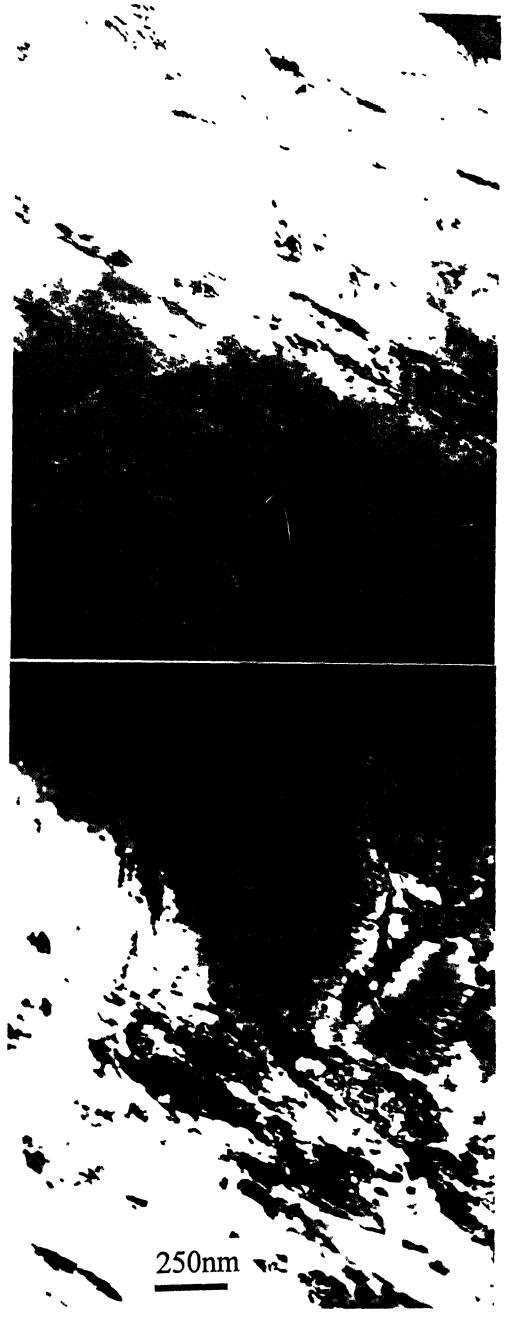

Figure 5.6 Transmission electron micrograph of steel annealed at 450°C for 2 hours

5.2. Effect of Annealing on Mechanical Properties

5.2.1. Effect of Annealing Temperature and Time on Hardness

The microstructure resulted after thermomechanical treatment followed by two-step cooling has the hardness of 52–56 Rc. Effect of annealing temperature and time on hardness can be seen in Figure 5.7. For all the four annealing temperatures, initial fall in hardness value is observed, after attending a lowest value it increases with annealing time and shown no significant change in macrohardness values between the annealing periods from 1.5 hours to 2.5 hours. Annealing at 450°C temperature has resulted in the high hardness values compared to other annealing temperatures.

The high hardness of thermomechanically treated two step cooled steel is due to the super saturated ferrite and bainitic/martensitic hard phases, as shown in Figure 5.2. The initial decrease in hardness on annealing is because of recovery process, and tempering of bainite/martensite. On annealing the bainite/martensite, formed during second step of cooling, starts dissociating into soft ferrite phase and carbides, secondly the annihilation of dislocations during recovery process reducers the dislocation density which resulted from the TMT. No appreciable influence of annealing time on hardness, in the time range of 1.5 hours to 2.5 hours, can be attributed to the two mutually counteracting processes. First, tempering of bainite/martensite and recovery process which reduces the hardness. Second, precipitation of V(C, N) particles in supersaturated ferrite [Gonzaliz, 1997] increases the resistance to dislocation movement.

5.2.2 Effect of Annealing Temperature and Time on Monotonic Properties

The tensile properties (0.2% offset yield strength σ_{ys}, ultimate tensile strength σ_{uts}, percentage elongation and percentage reduction in area, strain hardening exponent and strength coefficient K) of two step cooled, two step cooled plus annealed at four different temperatures and times are shown in Table 5.1. The engineering stress- strain curves for the two conditions for which low cycle fatigue testing was done is shown in the Figure 5.7

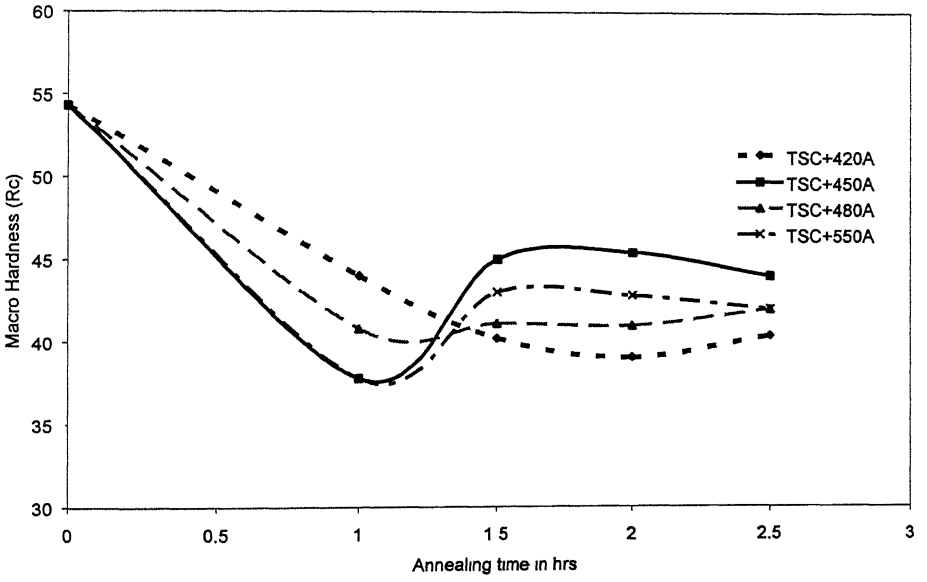

Figure 5.7 Effect of time and temperature on macro hardness of TSC microstructure

Table 5.1 Showing the tensile test results.

Condition Two Step Cooled (TSC)	Ultimate tensile strength, MPa (UTS).	Yield strength, MPa. (Y.S)	Percentage Elongation (%e)	Percentage Reduction in area (%z)	Strain Hardening Exponent (n)	Strength Coefficient, MPa. (K)
TSC	1878	1460	1.12	0.62	0.315	9549
420°CA,1Hr.	1283	1016	6.6	24	0.14	1995
450°CA,1Hr.	1208	965	8.3	32	0.149	1849
480°CA,1Hr.	1206	973	11.2	35	0.086	1778
420°CA,2Hr.	1468	1069	8.0	21	0.210	2775
450°CA,2Hr.	1432	1296	9.0	42	0.071	1914
480°CA,2Hr.	1330	1208	10	42	0.062	1728
550°CA,2Hr.	1245	1150	11	45	0.064	1581

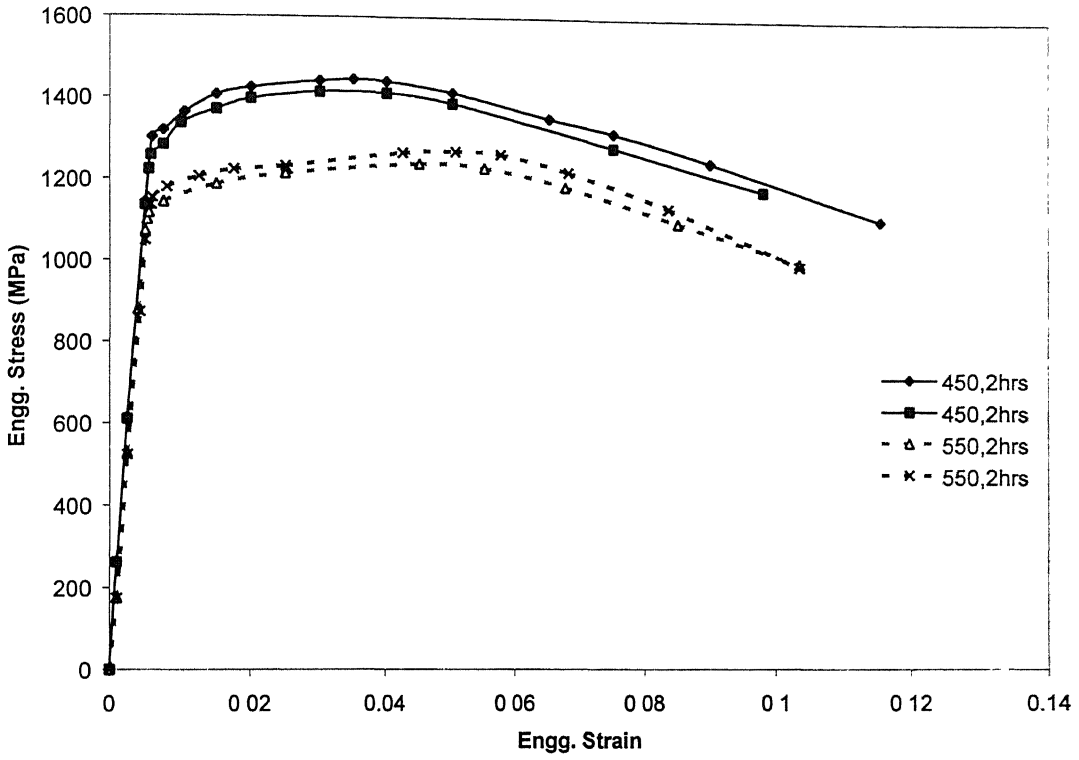

Figure 5.8 Engineering stress vs strain plot for 450 (A, 2) and 550 (A, 2) conditions

Figure 5.9 & 5.10 shows the variation in tensile properties with annealing temperature and annealing time. A decreasing trend in ultimate tensile strength (UTS) is seen with the increase in annealing temperature but it increases with the time of annealing for the same temperature. In contrast to the UTS, 0.2% offset yield point (YS) first increases with annealing temperature then gradually decreases with increase in temperature. The effect of annealing time on YS remains same as that on UTS but higher (34%) rise in YS is observed at 450°C annealing temperature. Annealing time and temperature have no significant effect on the percentage elongation but on the other hand significant increase, as high as 30% at 450°C annealing temperature, in percentage reduction in area is observed on increasing annealing time for the same temperature of annealing. Annealing at 450°C for 2 hours results in the best combination of strength and ductility, Table 5.1.

Decrease in UTS with annealing temperature is due to the tempering of bainite/martensitic hard phase which decomposes into ferrite and carbide. As discussed earlier the dissociation of austenite into ferrite and carbide in this temperature range increases the ferrite fraction of the steel, Figure 5.2 and 5.3. The improvement in % reduction in area with annealing time is due the larger extent dissociation of austenite which is apparent form the microstructures annealed for different times at same temperature. The effect of time on strength could be attributed to the precipitation of vanadium carbide/carbonitride which has taken place in ferrite can be seen in the transmission electron micrograph, Figure 5.27. Significant change observed of annealing time is due to the formation of coherent precipitates with the ferrite matrix which provide high resistance to the dislocation motion.

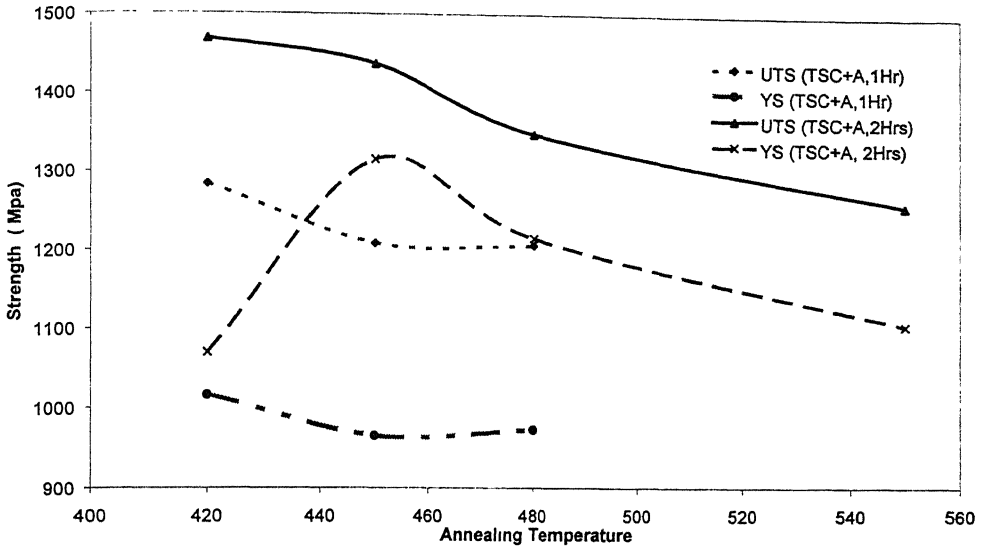

Figure 5.9 Effect of time and temperature of annealing on tensile properties

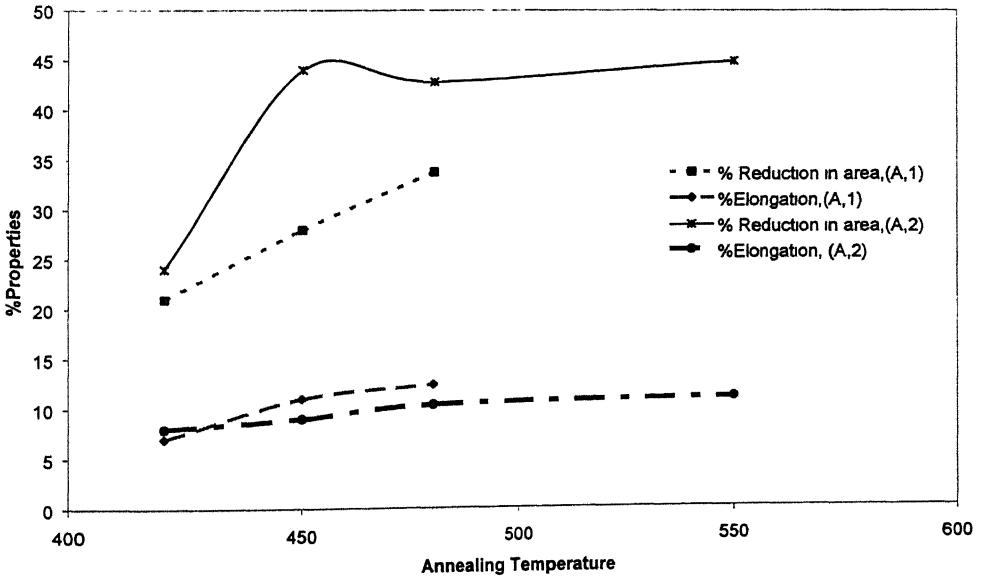

Figure 5.9. Effect of time and temperature on the % elongation and % reduction in area

5.4 Low Cycle Fatigue Response

5.4.1 Cyclic Stress /Strain Response

Monotonic and cyclic stress/strain curves for the two treatments are shown in Figure 5.11. Both the conditions i.e. TSC + 450°C and TSC + 550°C annealed have shown softening all the way till fracture. Figure 5.12 shows stress amplitude plotted against the number of reversals for the two conditions at representative strain amplitude. The softening was seen in all range of strains. Values of monotonic strain hardening exponent of the steel for the two annealing conditions, i.e. at 450 (A, 2) and 550 (A, 2), are shown in Table 5.1. It can be seen that both these values are low, i.e. 0.071 and 0.064 respectively. It has been suggested that the cyclic softening is associated with low strain hardening exponent (< 0.15) [Manson, 1963; Dieter, 1988]. The softening behavior of the steel for these two annealing conditions was therefore found to be along the expected line.

Reasons which could result in softening have been identified are unpinning of dislocations, shearing of precipitates, disordering of ordered precipitates, reversion or re-dissolution of precipitates and formation of persistent slip bands (PSBs) [Suresh, 1991]. TEM micrographs of samples undergone 0.5% and 1.1% strain amplitudes respectively were examined and have been shown in Section 5.6. The initial stages of cell formation were observed. Unpinning of some dislocations during first half cycle in individual isolated grains may therefore be the reason for continuous softening behavior of the steel during LCF testing. And this keeps increasing on subsequent cycles. Hence, the material is in the plastically inhomogeneous condition, because beside the plastically deformed

grains there are those that behave essentially elastic. The increase in plastic deformation $\Delta\varepsilon_p/2$ is result of increase in number of such isolated grains with the number of cycle.

5.4.2 Cyclic Strain/Life Response

Figure 5.13 shows strain/life plot for the two treatments. From the linear portion of the elastic and plastic curves, the fatigue strength coefficient (σ_f'), fatigue strength exponent (b), fatigue ductility coefficient (ε_f') and fatigue ductility exponent (c) were determined. Values of cyclic strain hardening exponent (n′) and cyclic strength coefficient (K′) were also obtained from plot of $\text{Log}(\Delta\sigma/2)$ vs $\text{Log}(\Delta\varepsilon_p/2)$ are the stress range and plastic strain range at about half the fatigue life. The definition and values of n′, K, σ_f', b, c and ε_f' are given in Table 5.2 and Table 5.3 respectively. The observed value of b and c for both the treatment are in reasonable agreement with those calculated from the values of n′ using equation proposed by Tomkins [Tomkins, 1968].

At high plastic strains, the ductility is the prime consideration governing the fatigue resistance. Cracks are found to initiate relatively early in the life and crack growth is the dominant failure mode. Conversely, at low plastic strain amplitudes, strength governs failure and crack initiation becomes the increasingly dominant event. The numbers of reversals $(2N_f)_t$ at which the elastic and plastic strain are equal is called the transition life [Suresh, 1991].

$$(2N_f)_t = (\varepsilon_f' E/ \sigma_f')^{1/(b-c)} \qquad 5.1$$

Transition life for the two treatments is given in Table 5.3. At short fatigue lives, i.e. when $(2N_f) < (2N_f)_t$, the plastic strain amplitude is more dominant than the elastic strain amplitude and the fatigue life is controlled by ductility. At long fatigue lives, i.e. when $(2N_f) > (2N_f)_t$, the fatigue life is dictated by rupture strength. Long life resistance increases with increase in strength. Thus, optimizing the overall fatigue properties requires a judicious balance between strength and ductility.

Total strain/ life and plastic strain/ life plots are compared in Figure 5.14 and Figure 5.15 respectively. It is seen that the steel in both the treatment obeys the Coffin-Manson law.

(a)

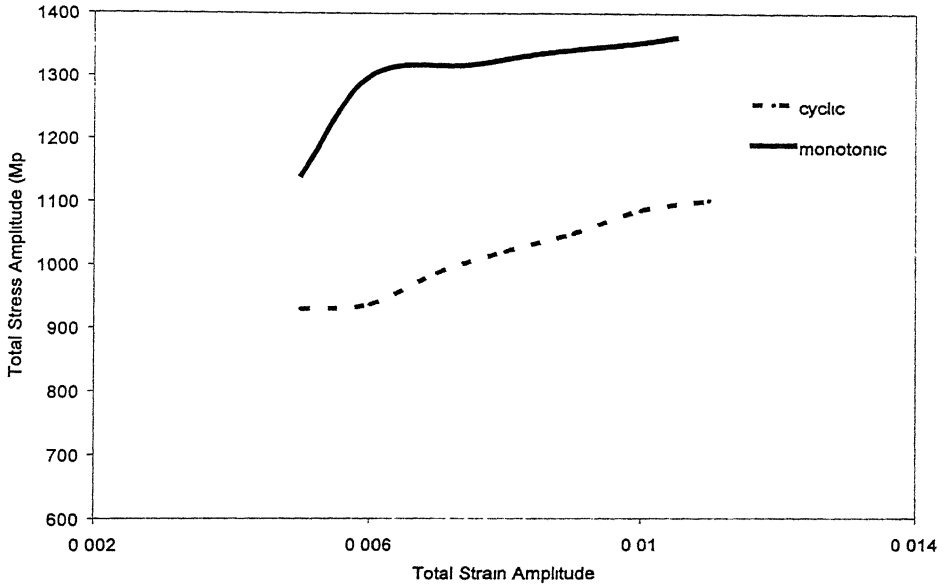

(b)

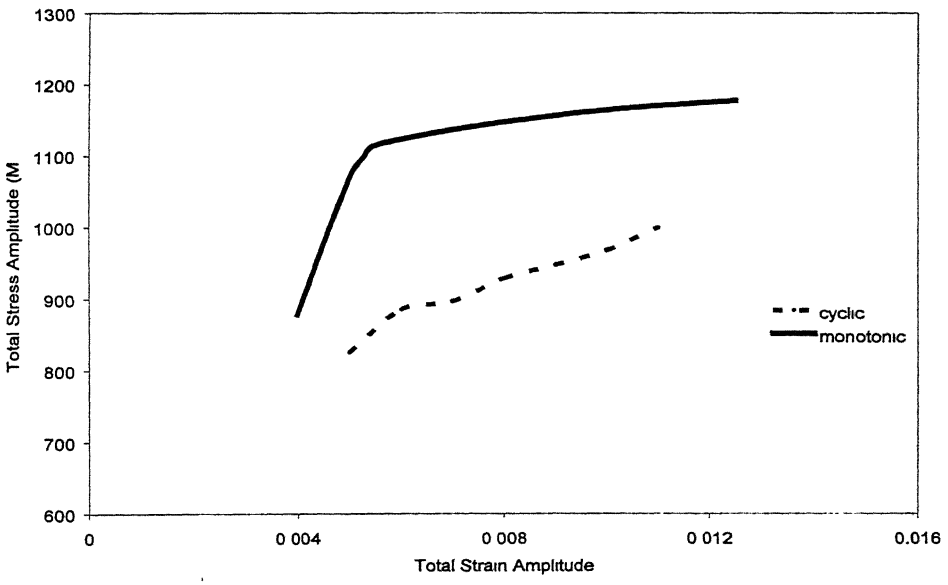

Figure 5.11 (a) Cyclic and monotonic stress strain plot for 450 (A, 2) condition, (b) cyclic and monotonic stress strain plot for 550 (A, 2) condition.

(a)

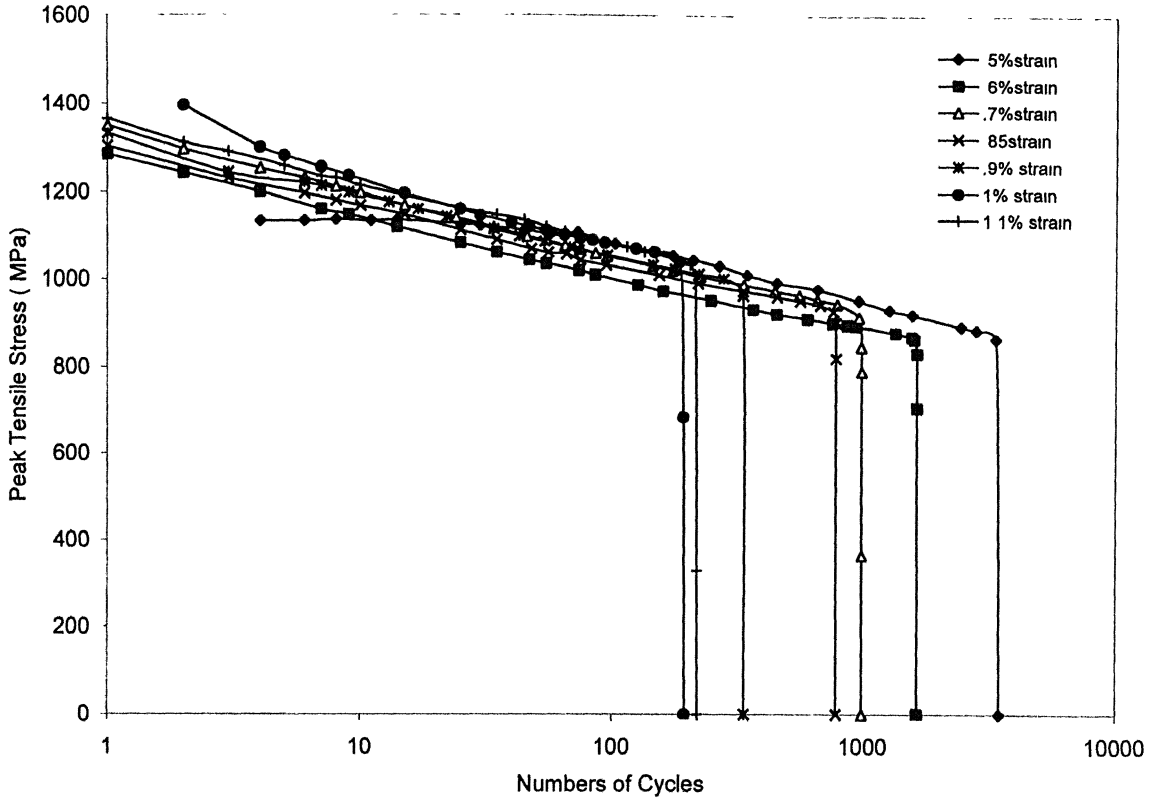
1600
1400
1200
1000
800
600
400
200
0
Peak Tensile Stress (MPa)
1
10
100
1000
10000
Numbers of Cycles
5%strain
6%strain
.7%strain
85strain
.9% strain
1% strain
1 1% strain

Table 5.2 Definitions of fatigue exponents and coefficient

Properties	Definition
Cyclic strain hardening exponent, n′	Exponent of true steady-state stress amplitude and plastic strain amplitude relationship, i.e. $\Delta\sigma/2=K'(\Delta\varepsilon_p'/2)^{n'}$ (taken as the slope of $\log(\Delta\sigma/2)/\log(\Delta\varepsilon_p'/2)$ plot)
Cyclic strength coefficient, K′(MPa)	True steady state cyclic stress required to cause a true plastic strain of unit in the above equation
Cyclic ductility coefficient, ε_f'	True cyclic strain required to cause failure in one reversal (taken as antilog of the intercept of: $\log(\Delta\varepsilon_p/2)$ /$\log 2N_f'$ plot at $2N_f=1$
Cyclic ductility exponent, c	Power to which the life in reversals must be raised to be proportional to the plastic strain amplitude (taken as the slope of the $\log(\Delta\varepsilon_p/2)/\log 2N_f$ plot)
Cyclic strength coefficient, σ_f' (MPa)	True cyclic stress required to cause fracture in one reversal (taken as antilog of the intercept of: $\log(\Delta\sigma/2)$ /$\log 2N_f'$ plot at $2N_f=1$)
Cyclic strength exponent, b	Power to which the life in reversals must be raised to be proportional to stress amplitude (taken as the slope of the $\log(\Delta\sigma/2)$ /$\log 2N_f$ plot)

Table 5.3 Low cycle fatigue test results

Properties	Material Condition TSC	
	450 (A, 2)	**550 (A, 2)**
Fatigue ductility coefficient, ε'	0.711	0.973
Cyclic strain hardening exponent, n′	0.098	0.0814
Fatigue ductility exponent, c	-0.795	-0.853
$c = -1/(1+2n')$ *	-0.836	-0.859
$c = -1/(1+5n')$ **	-0.67	-0.71
Fatigue strength exponent, b	-0.0616	-0.0724
$b = -n'/(1+2n')$ *	-0.0819	-0.07
$b = -n'/(1+5n')$ **	-0.0657	-0.057
Cyclic yield strength MPa	736	680
Fatigue strength coefficient MPa	1315	1220
Strength coefficient MPa (K′)	1817.7	1489.5
Transition life $(2N_f)_t$	538	462

* Expected using Tomkins model

** Expected using Morrow model

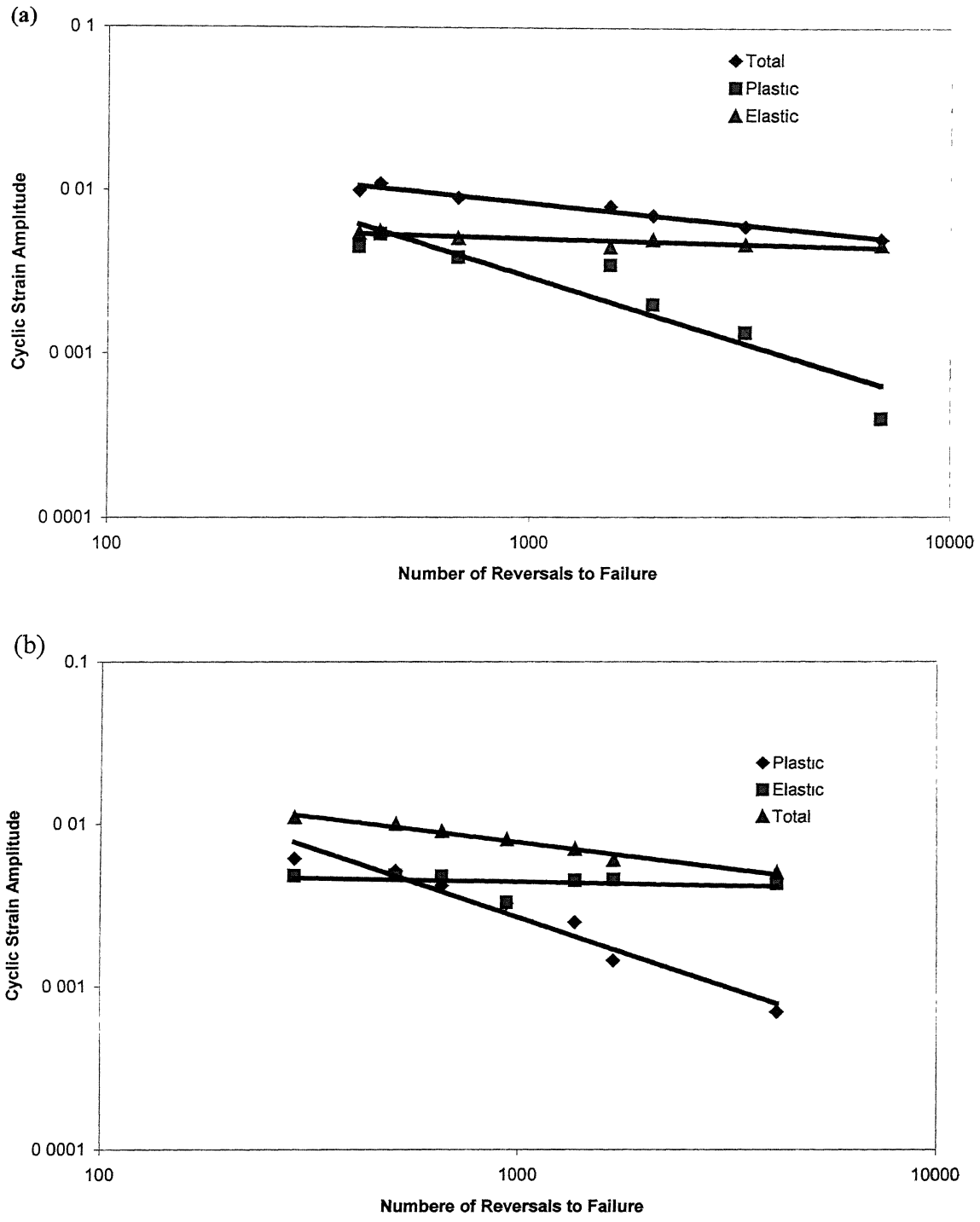

Figure 5.13 (a) Cyclic total, elastic and plastic strain amplitudes as a function of the number of load reversals to failure for 450 (A, 2), (b) Cyclic total, elastic and plastic strain amplitudes as a function of the number of load reversals to failure for 550 (A, 2)

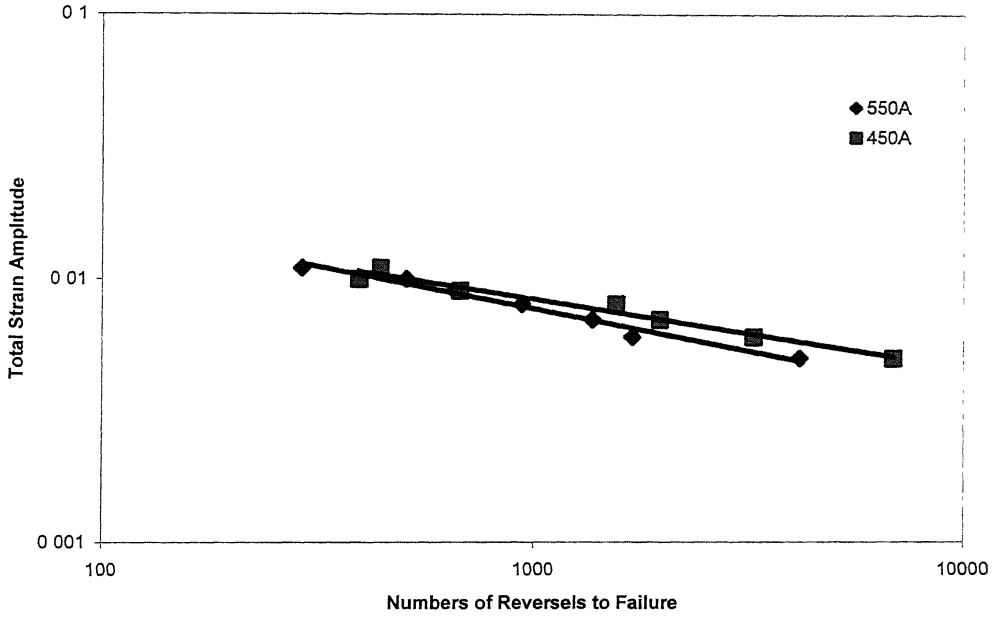

Figure 5.14 Total strain amplitude as a function of number of reversals to failure for 450 (A, 2) and 550 (A, 2) conditions

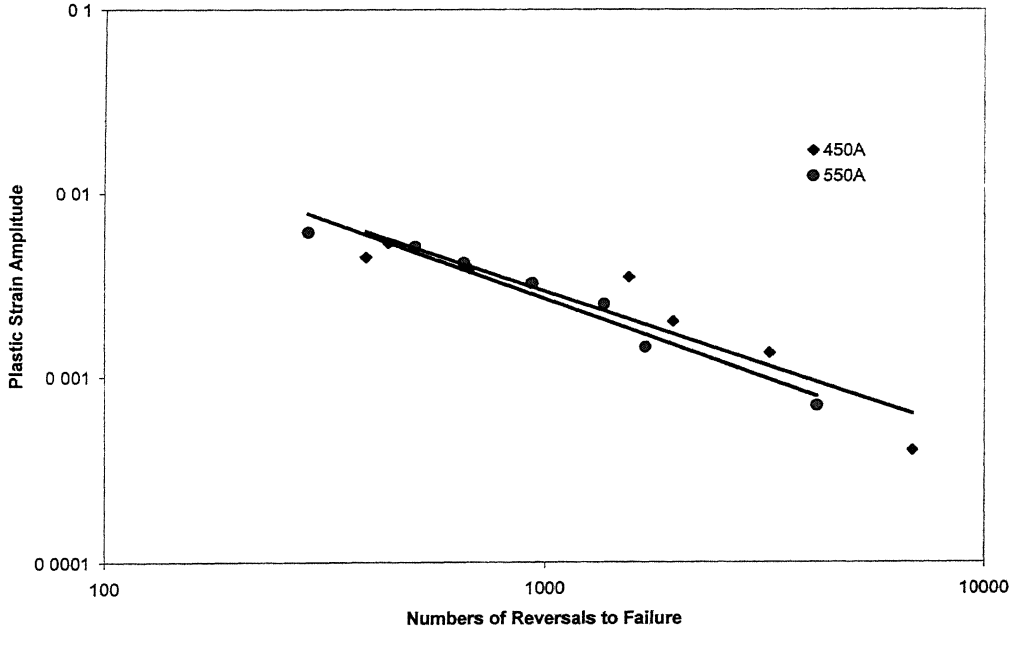

Figure 5.15 Coffin-Manson plots for 450 (A, 2) and 550 (A, 2) conditions

5.4.3 Life Assessment

Several empirical methods are designed to approximate the fatigue life data using tensile properties. One such method, the modified universal slopes (MUS) method (Muralitharan, 1988; Sarma, 1998) has been suggested to give reliable results. The MUS equation is given by

$$\Delta\varepsilon_t = 1.17\,(\sigma_b/E)^{0.832}\,N_f^{-0.09} + 0.0266\,\varepsilon_f^{0.155}\,(\sigma_b/E)^{-0.53}\,N_f^{-0.053} \qquad 5.2$$

where $\Delta\varepsilon_t$ is the total strain amplitude, σ_b is the ultimate tensile strength, N_f is the number of cycles to failure. Using continuum mechanics approach and assuming that crack propagation consumes most of the low cycle fatigue life, Tomkins on the other hand proposed

$$N_f = \left(\mathrm{Ln}\,(a_f/a_o)\right) / \left((\sec(\pi\sigma/2\sigma_b) - 1)\,\Delta\varepsilon_p/2\right) \qquad 5.3$$

Where a_o and a_f are the initial and final crack length respectively. Figure 5.16 shows the comparison between the experimental data and results predicted by the Tomkins' model. It is seen that Tomkin's model slightly overestimates the life (two times at higher strains and 1.5 times at low strains) for 450 (A, 2) condition. In contrast, the MUS model overestimates the life as high as a factor of 30 times, Figure 5.16. As shown in Figure 5.17, the same trend is also observed with the 550 (A, 2) condition. These results highlight the limitation of the two empirical approaches and emphasize that high tensile strength need not always enhance the fatigue life.

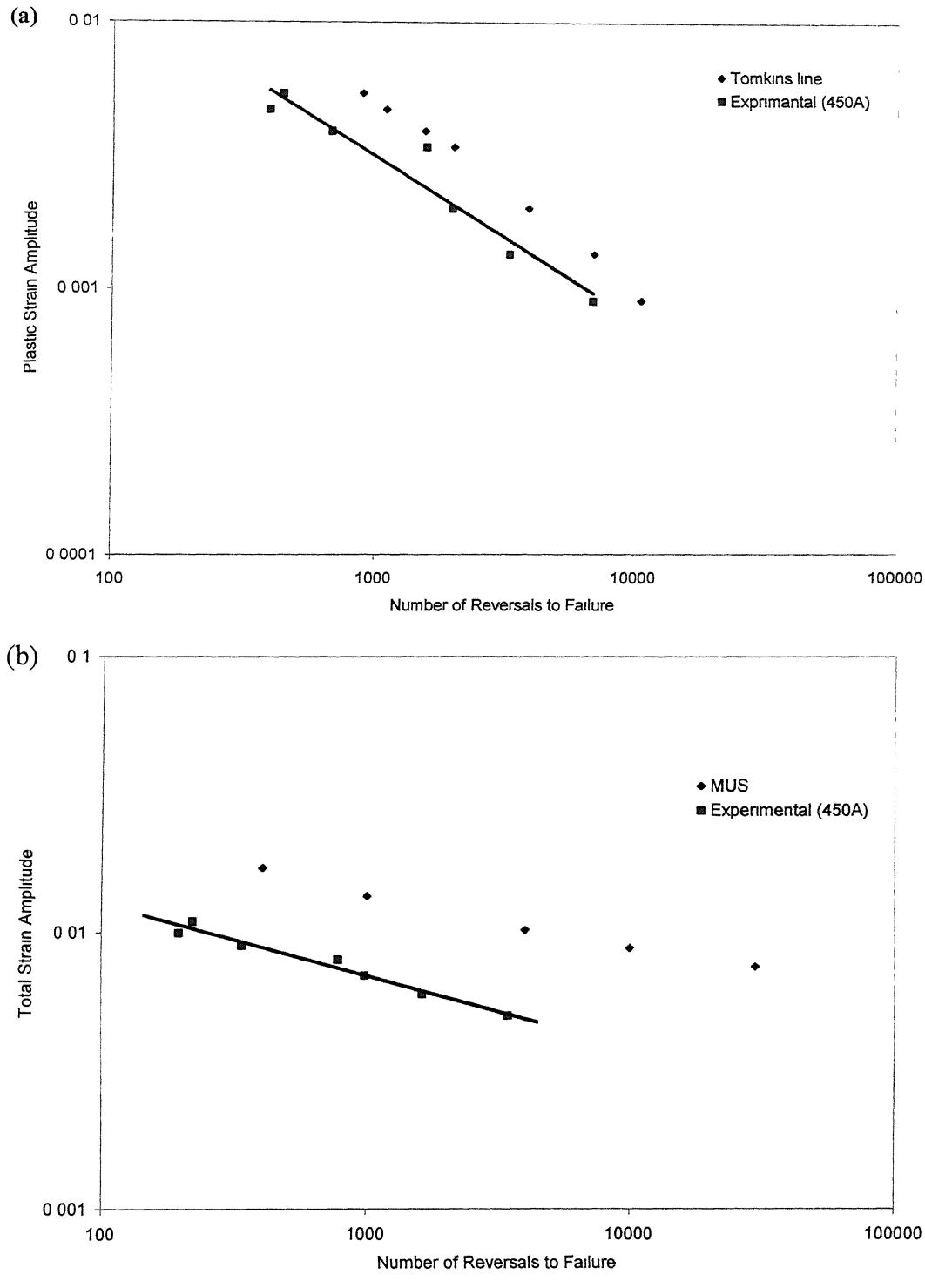

Figure 5.16 (a) Life prediction by Tomkins' model, (b) Life prediction by MUS model for 450 (A, 2) condition

(a)

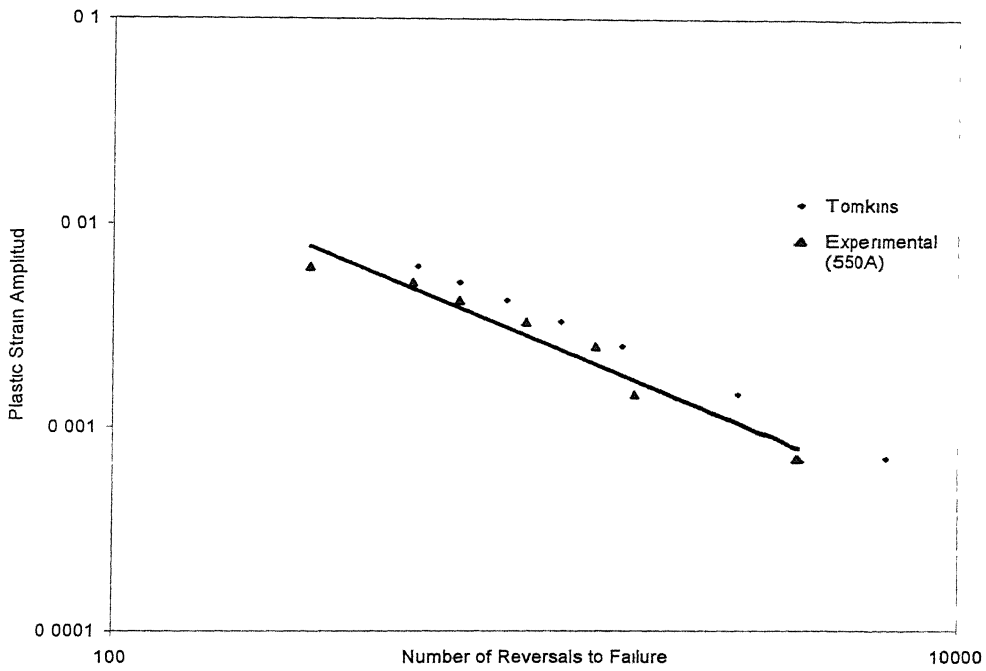

(b)

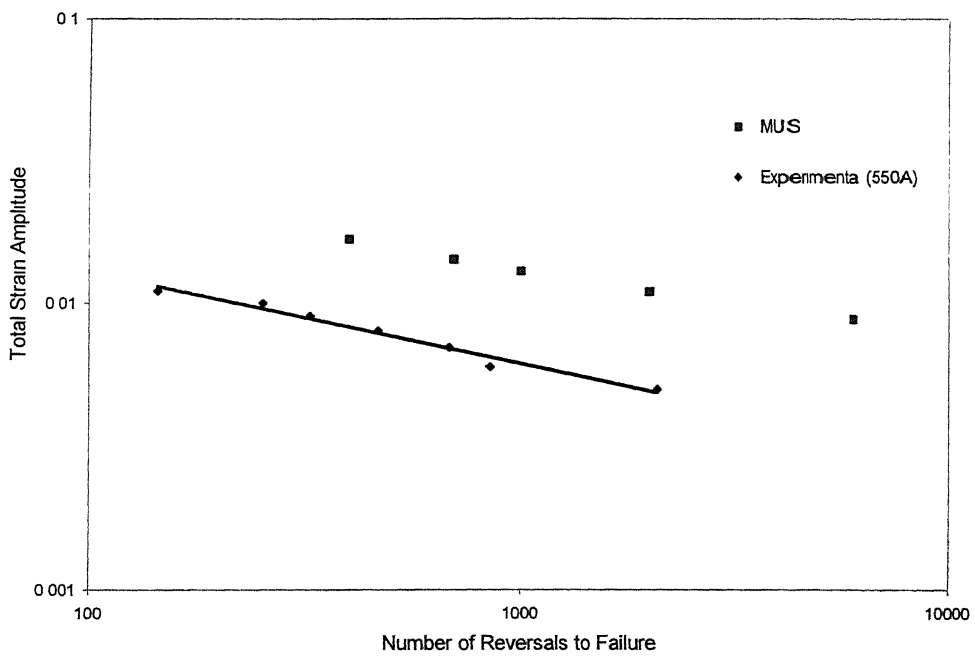

Figure5.17 (a) Life prediction by Tomkins' model (b) Life prediction by MUS model for 550 (A, 2) condition

5.5 Fatigue Crack Propagation test

Results of fatigue crack growth rate tests for 550 (A, 2.) condition at two different stress ratios (R=0.1 and R=0.4) are shown in the Figure 5.18. Intermediate and higher crack growth rate regime can be seen in the da/dN vs. ΔK plot. Though a full low crack growth rate regime (near threshold) could not be established but a trend can be seen. The data obtained, in the mid-range, for both the stress ratios were found to confirm the power law relationship proposed by Paris. The scaling constants are given in the Table 5.4, where m is the exponent term.

At high ΔK values, the fatigue crack growth rates are higher than those observed in the Paris regime. This is because of K_{max} approaches the fracture toughness of the material [Suresh, 1998]. Effect of stress ratio in the midrange of fatigue crack growth plot is insignificant as the slopes are comparable but it effect can be seen in the higher ΔK region, where the R=0.4 has shown high crack growth rate compared to one at R=0.1. The enhanced influence of stress ratio in the higher ΔK region is a consequence of the critical condition that the maximum stress intensity factor value for the fatigue cycle, K_{max}, approaches K_{1C} of the material.

$$K_{max} = \Delta K/(1-R) \rightarrow K_{1C}, \qquad 5.4$$

Since the ΔK value, at which K_{max} begins to approach K_{1C}, is lower for high R values the catastrophic fatigue failure occurs at lower ΔK values with an increase in stress ratio.

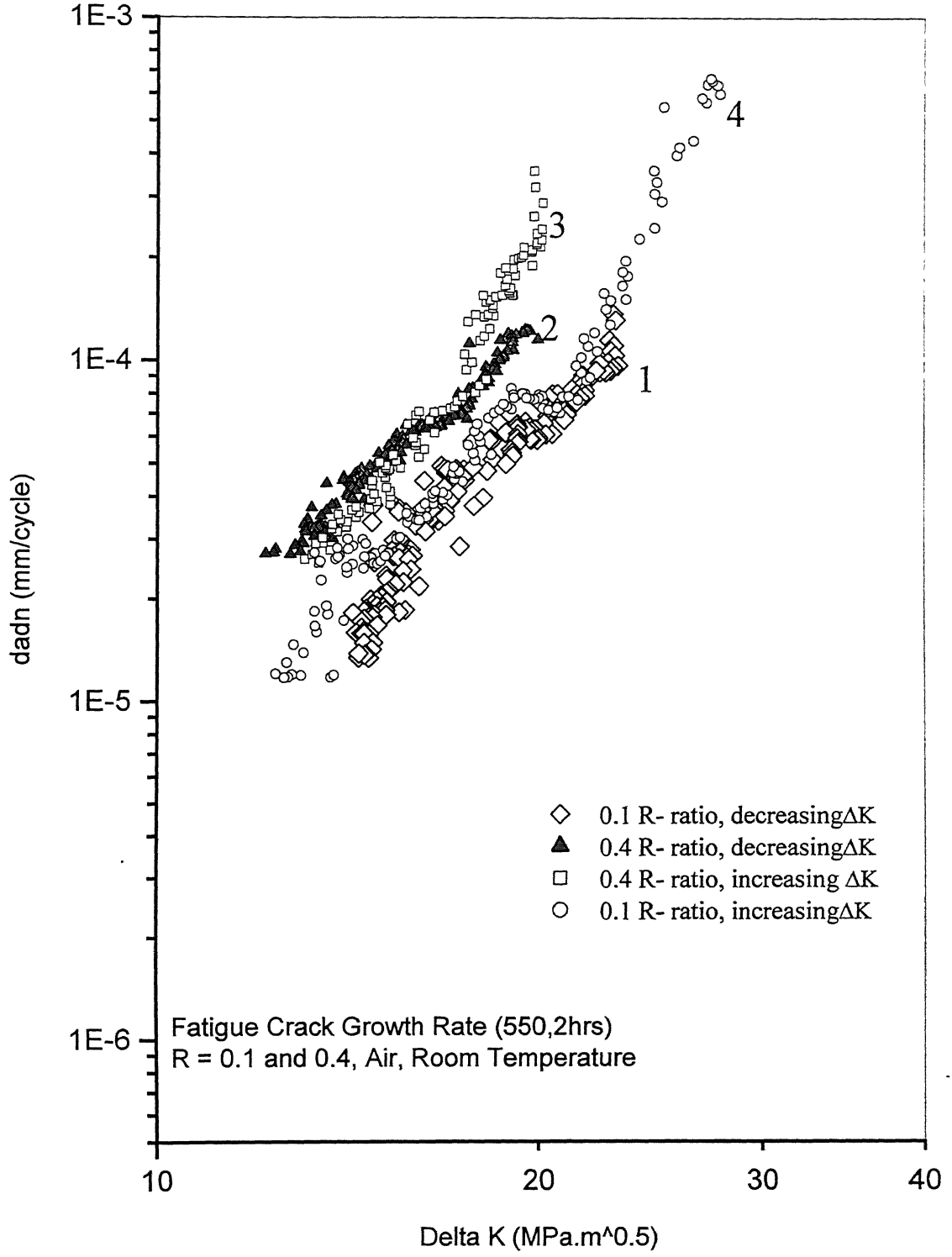
1E-3
1E-4
1E-5
1E-6
dadn (mm/cycle)
10
20
30
40
Delta K (MPa.m^0.5)
1
2
3
4
0.1 R- ratio, decreasingΔK
0.4 R- ratio, decreasingΔK
0.4 R- ratio, increasing ΔK
0.1 R- ratio, increasingΔK
Fatigue Crack Growth Rate (550,2hrs)
R = 0.1 and 0.4, Air, Room Temperature

Table 5.4 Paris scaling constants

Load ratio	C (mm/cycle)	m
0.1	4.809×10^{-9}	2.94
0.4	7.64×10^{-9}	3.24

5.4.4 Fractography of LCF and FCGR Tested Samples

Fracture surface of samples tested in the low cycle fatigue regime and crack propagation test were examined for sites of crack initiation and mode of crack propagation. As shown in the Figure 5.19, both the conditions, i.e. 450 (A, 2) and 550(A, 2) revealed that the crack initiation took place predominantly near the surface. Surface roughness and protrusions cause localization of stress and plastic strain, which, in turn, could result in initiation of microcracks. Stage II crack propagation takes place predominantly through microvoid growth and coalescence process. As seen in the Figure 5.20, microvoid initiation stage is attributed to the interfacial failure between inclusion/ precipitate particle and the surrounding matrix. The final failure involves the coalescence of count less microvoids, Figure 5.21. At higher strain levels intergranular cleavage is also seen (Figure 5.22). The size of second phase particle causing initiation of microvoid is around 2-3μm. Void initiation, therefore, can be attributed to inclusion-matrix decohesion or cracking, depending upon the relative strength of the inclusion and the matrix. The VC particles are known to be very hard and therefore cracking of them is not expected. Though no evidence is yet available in the present study, fine VC particles in the steel are also expected to be the void nucleating particles. Striated crack growth, indication of stage-II fatigue crack growth, is also observed in both the condition at all

strain levels Figure 5.23. Secondary cracks, which resulted from the large plastic zone in front of crack tip, are also observed.

Figure 5.24 shows the ductile striations which are typical characteristics of intermediate crack growth are resulted from the crack blunting and re-sharpening during cyclic loading. The transgranular cleavage fracture resulted due to high ΔK can be seen in the Figure 5.25.

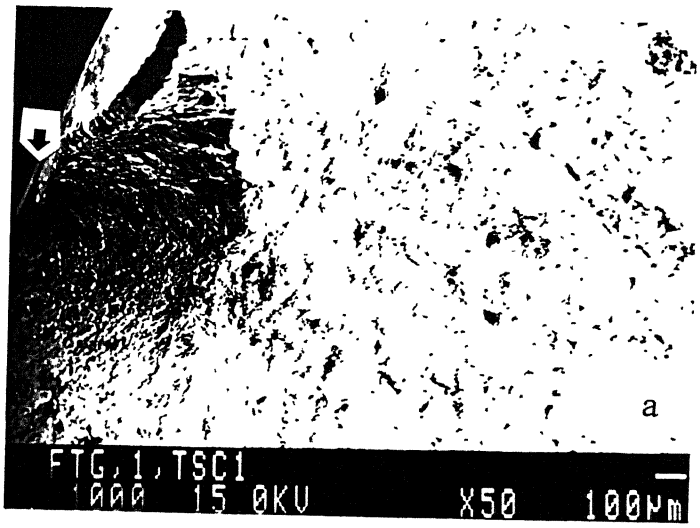

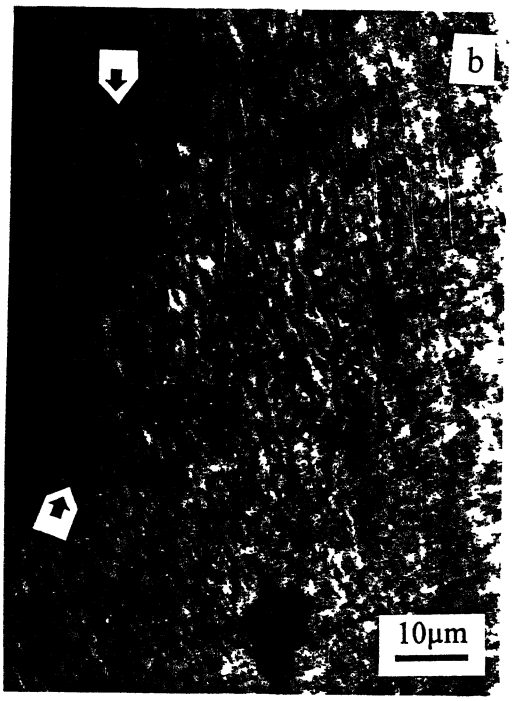

Figure 5.19 Fractograph of low cycle fatigue failed samples showing crack initiation at the surface (a) fracture surface (0.5% strain amplitude, 450 (A, 2) condition) (b) vertical section near the fracture surface (1% strain amplitude, 550 (A, 2) condition).

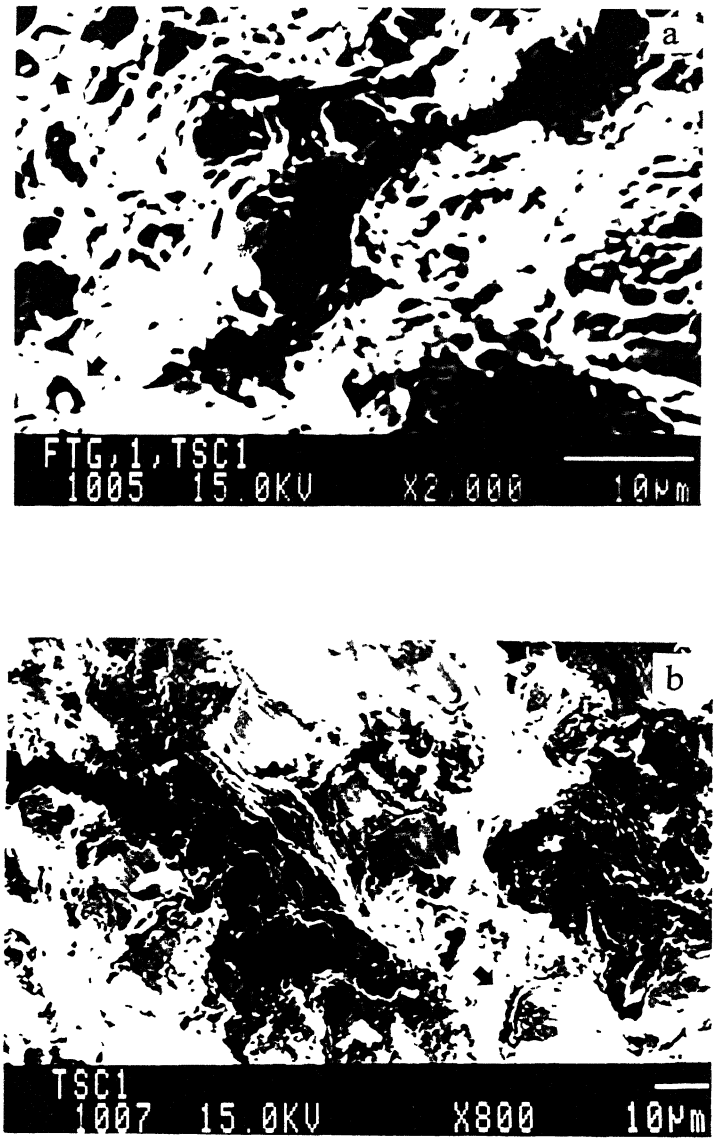

Figure 5.20 Fractographs showing the microvoid initiation at the interface of second phase and matrix (a) 1% strain amplitude, 550 (A, 2) condition (b) 0.5% strain amplitude, 450 (A, 2) condition.

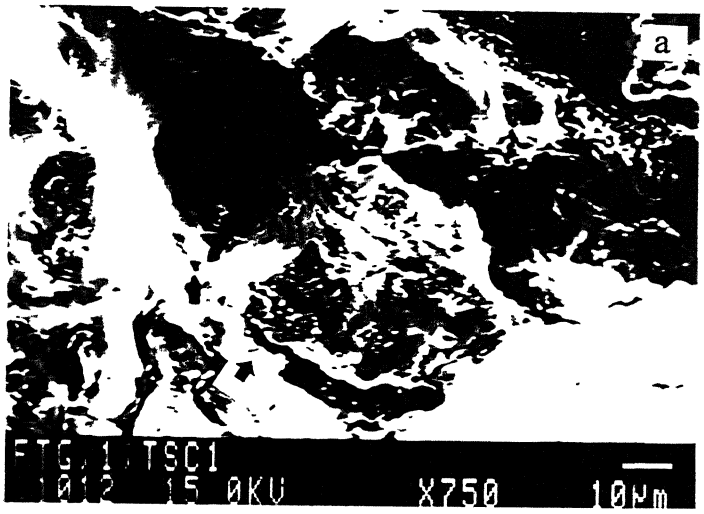
a
FIG,1,TSC1
0012 15.0KV X750 10μm

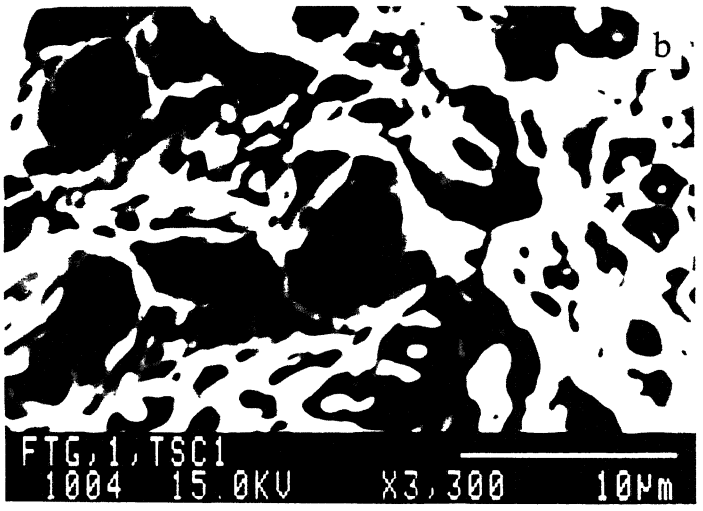
b
FIG,1,TSC1
1004 15.0KV X3,300 10μm

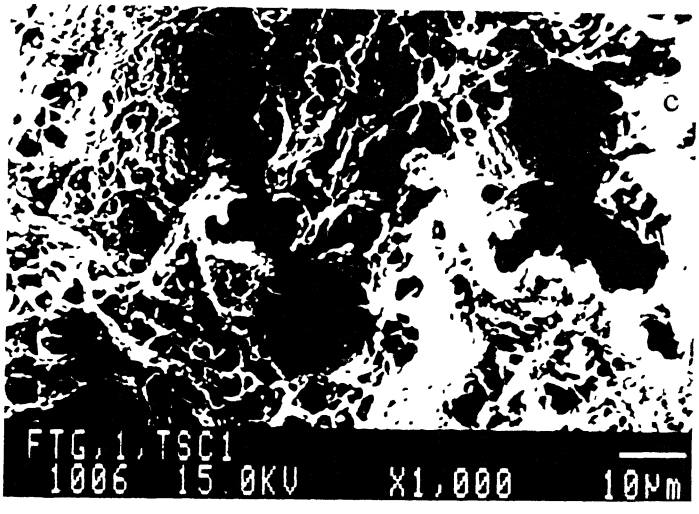

Figure 5.21 Fractographs showing the microcrack growth and coalescence (a) second phase particle-matrix interface failure and growth of crack (1% strain amplitude, 550 (A, 2) condition (b) microvoid coalescence (0.5% strain amplitude, 550 (A, 2) condition) (c) second phase- matrix interface failure and microvoid coalescence (1% strain amplitude, 450 (A, 2) condition

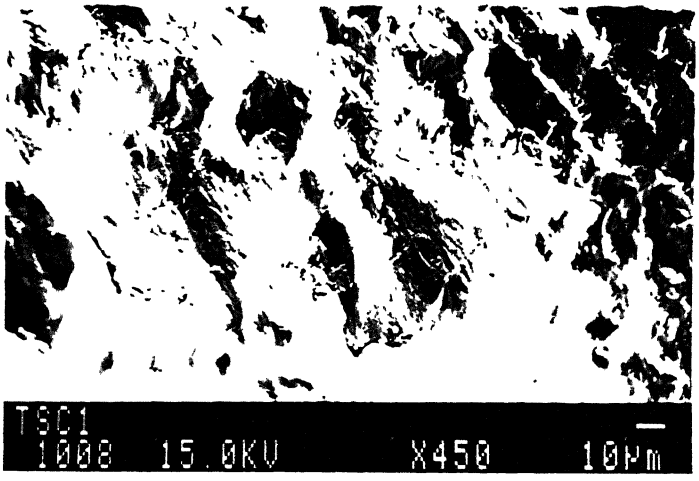

Figure 5.22 Fractograph showing the intergranular cleavage fracture at 1% strain amplitude, 450 (A, 2) condition.

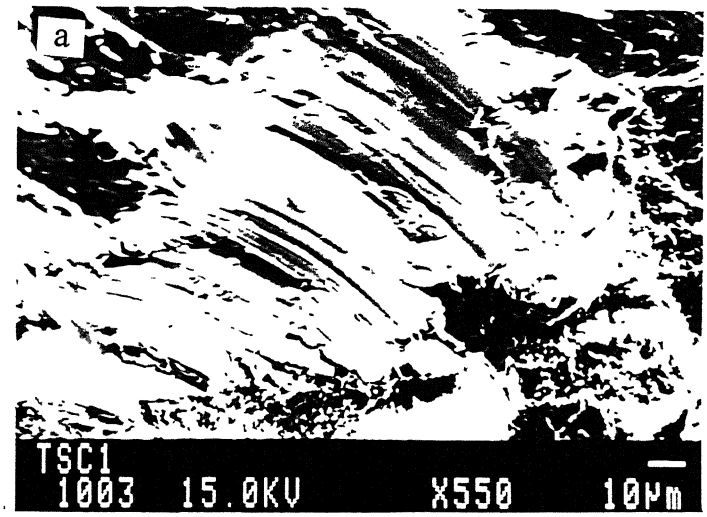
a
TSC1
1003 15.0KV X550 10µm

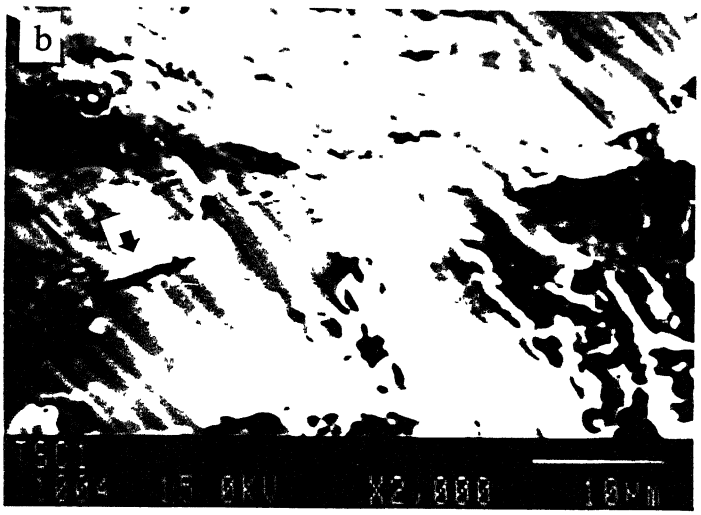
b

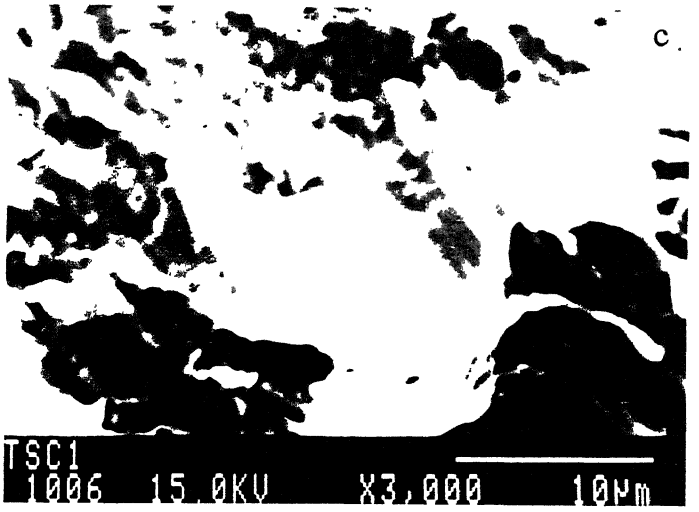

Figure 5.23 Fractograph showing striations (a) 0.5% strain amplitude, 550 (A, 2) condition (b) secondary crack (arrowed) 1% strain amplitude, 550 (A, 2) condition (c) 1% strain amplitude, 450 (A, 2) condition

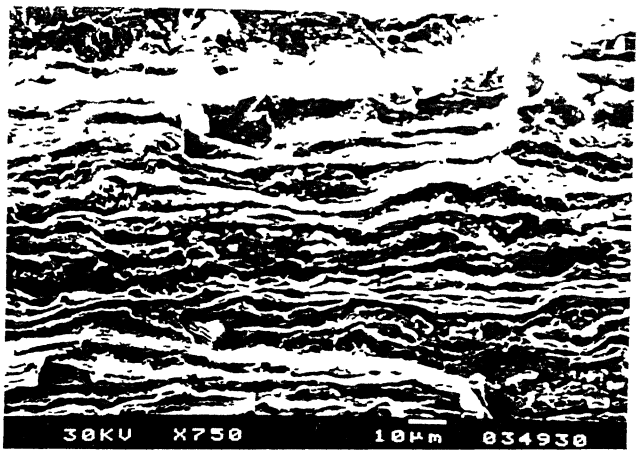

Figure 5.24 Fractograph showing the ductile striations formed during intermediate range, 550 (A, 2) condition (FCGR test.)

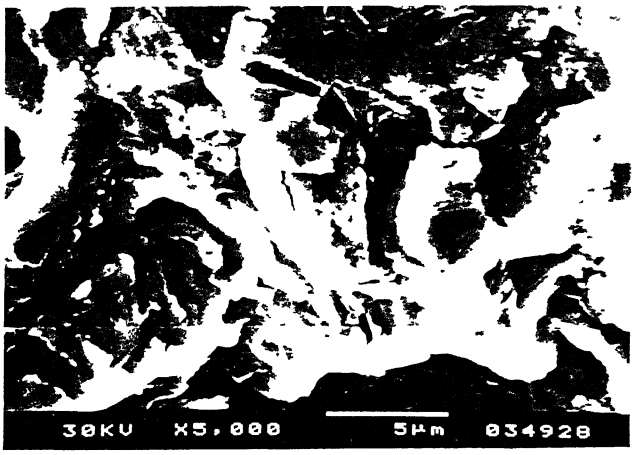

Figure 5.25 Fractograph showing the transgranular cleavage fracture, 550 (A, 2) condition (FCGR test)

5.6 Microstructural evolution during cyclic loading

In order to find out the response of the microstructure to cyclic loading, transmission electron microscopy was carried out samples (a) 450°C annealed for 2 hours (without cyclic loading), (b) 450°C annealed for 2 hours after cyclic loading at 0.6% and (c) 450°C annealed for 2 hours after cyclic loading at 1.1% strain levels. Figure 5.6 shows the TEM micrograph of 450 (A, 2) sample revealing the presence of the laths of ferrite and carbide in this condition. This microstructural state has relatively less dislocation density and the carbide precipitates can be seen in the micrograph. Figure 5.26 (sample undergone 0.6% strain amplitude) also shows the laths of ferrite and cementite. However, an increase in dislocation density in the ferrite laths can be seen which is due to cyclic loading at 0.6% strain. The microstructural damage in the form of fragmentation of cementite is also observed. The initial stages of cell formation are also observed which could be the reason for continuous softening behavior of the steel which is discussed in earlier section. At high strain (1.1%) level high dislocation density is comparatively higher than that at the strain amplitude of 0.6% and fragmentation of cementite laths is also more, Figure 5.27. The fine precipitates distributed in the ferrite lath which precipitated during the annealing and dislocation cell formation can be seen in the Figure 5.28. The ferrite and cementite are found to be related by Bagaryatskii orientation relationship. i.e.

$[1\bar{1}\bar{1}]_f \| [010]_c$,

$(0\bar{1}1)_f \| (100)_c$,

$(211)_f \| (001)_c$.

as shown in Figure5.29, this is typical of tempered martensite or lower bainite. The angle between the two twin related laths of ferrite is around 25 degrees. Which are shown in the diffracted pattern.

Figure 5.26 Transmission electron micrograph (sample undergone 0.6% strain amplitude) showing the ferrite lath and carbide precipitates (arrowed).

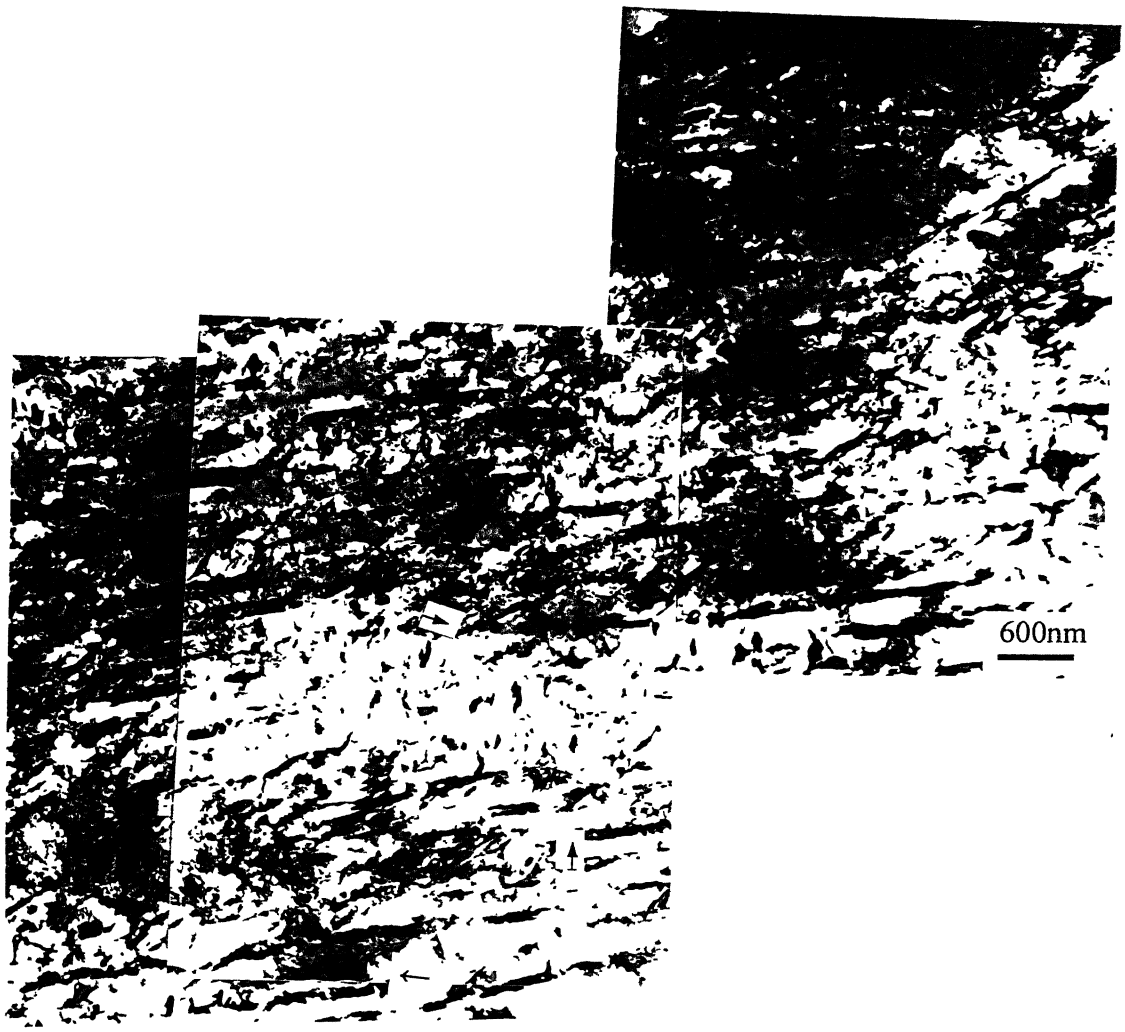

Figure 5.27 TEM micrograph showing the fragmented cementite at strain amplitude of 1.1%., high dislocation density (thin arrow) and shear band (thick arrow).

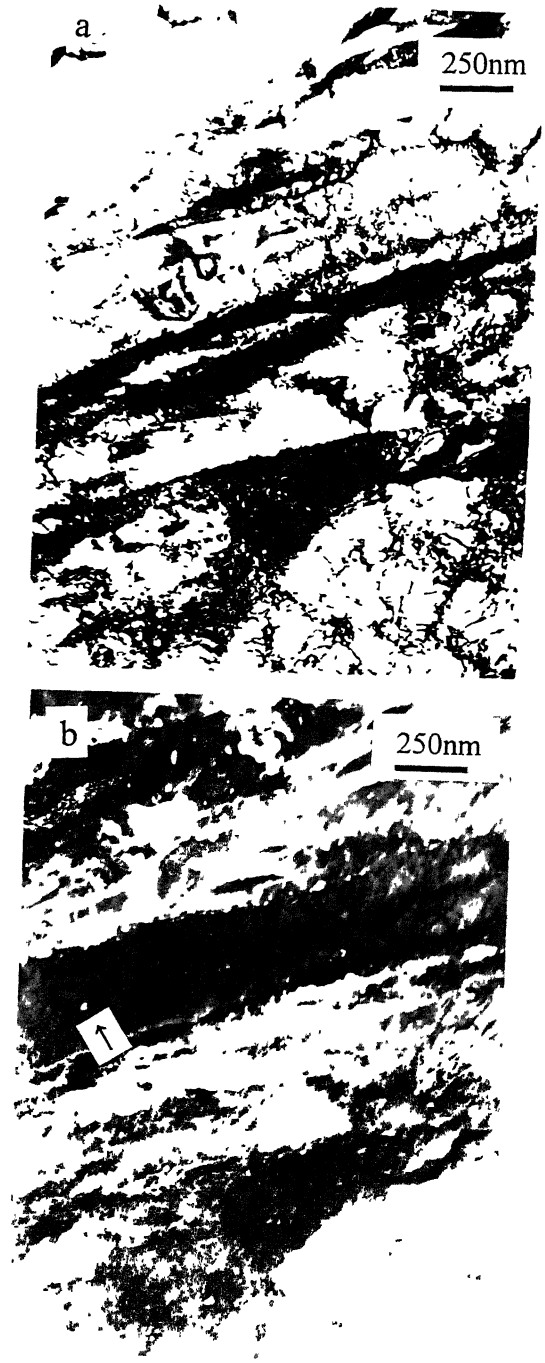

Figure 5.28 TEM micrograph showing dislocation cell formation (a) bright field image (b) corresponding area dark field image showing the fine precipitates (arrowed)

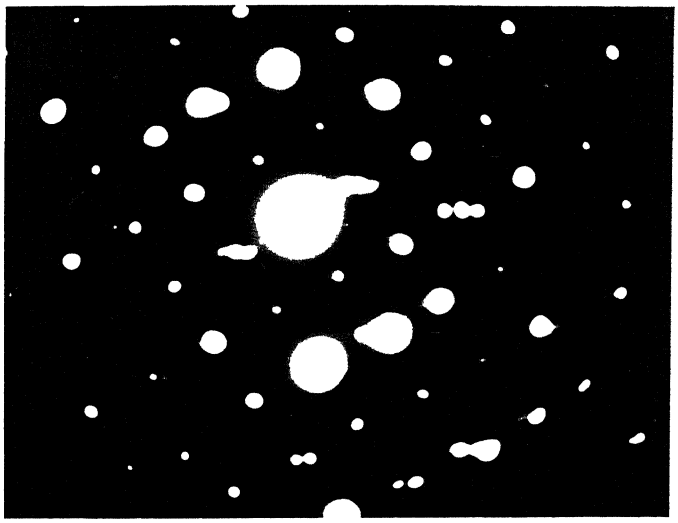

Figure 5.29 Diffraction pattern showing the orientation relationship between ferrite and cementite. (x) ferrite spot (•) ferrite spot (¤)showing cementite spots.

Chapter 6

CONCLUSIONS AND SUGGESTIONS FOR FUTURE WORK

6.1 Conclusions

The present investigation was undertaken to obtain (a) a muli-phase microstructure in the medium carbon microalloyed 38MnSiVS5 steel by a special thermomechanical working involving a two step cooling procedure and (b) to study the room temperature tensile as well as fatigue behaviour of the multi-phase structure. Investigations of the present study have resulted in the following conclusions

(1) Thermomechanical treatment involving forging at a finishing temperature of 900-850°C followed by the two-step cooling with (a) air cooling upto 700°C - 680°C after forging and (b) quenching in water immediately after air cooling results in a multi-phase microstructure consisting of bainite/martensite and isolated islands of ferrite phases. On subsequent annealing, this structure gives rise to tempered bainite/martensite. In addition, an increase in ferrite fraction is observed after annealing at all temperatures between 420°C to 550°C.

(2) No significant effect of annealing time on macro-hardness is observed during annealing period of 1.5 hours to 2.5 hours in the temperature range between 420°C to 550°C. In contrast, an appreciable improvement in strength and ductility is observed on increasing the annealing time from 1 hour to 2 hours at 420°C,

450°C as well as 480°C. It is found that the best combination of strength and ductility is obtained on annealing at 450°C for 2 hours.

(3) Thermomechanically treated 38MnSiVS5 steel involving two-step cooling after annealing at 450°C as well as 550°C respectively for a period of two hours shows cyclic softening till fracture for all strain levels.during low cycle fatigue tests. The cyclic yield strength and transition life are found to be more for the samples annealed at 450°C than the samples annealed at 550°C.

(4) An examination of fractured samples tested under low cycle fatigue shows that the cracks initiate due to its roughness at the sample surface, subsequently propogate and result in failure.

(5) Microstructural examination of the fractured samples shows that the interface between second phase particle and matrix gives rise to the nucleation of microvoids. Propagation of fatigue cracks in both the annealed conditions is found to be predominantly by the nucleation of microvoid growth and their coalescence. The examination of the tested samples under TEM shows that the cyclic loading results in the dislocation cell formation and fragmentation of cementite.

(6) Fatigue crack growth rate was found to be higher for higher stress ratio at high ΔK values.

6.2 Suggestion for Future Work

(1) Particle size and distribution of particle in the matrix should be studied and quantified. Efforts should be made to estimate the amount of strengthening in this microalloying steel.

(2) Effect of titanium/ niobium addition on high temperature thermomechanical treated steel should be determined.

(3) Stress controlled fatigue studies should be done to obtain the endurance limit and to generate the S-N curve.

(4) Fracture toughness measurements should be undertaken.

(5) Near threshold crack propagation studies can be done to determine the threshold values for the steel.

Chapter 7

REFRENCES

(1) Almen, J. O and Black, P. H. (1963), *Residual Stress and Fatigue in Matels*, New York, McGrow- Hill Book Co.

(2) Barsom, J., Imhof, E. J. and Rolf, S. T. (1970), *Engg. Fract. Mech.*, 2, 301.

(3) Dieter, I. E. (1988), *Mechanical Metallurgy*, New York, McGrow- Hill Book Co.

(4) Fourlaris, G. (1998), *Conference Microlloying in Steels*, Switzerland, Trans. Tech. Publications Ltd., 427.

(5) Farsetti,P and Blarasin, A (1988*), Int. J. Fatigue*,10 (3), 153.

(6) Flecteher, E.E (1979), MCIC Report/March

(7) Fuchs, H. O. and Stephens, R. I. (1977), *Metal Fatigue in Engineering.* London: Cambridge.

(8) Gough, H. J. (1933), *Test. Mater.* Proc., 33, 3.

(9) Kasper, R., Gonzalez, I. B., Richter, J., NuBbaum, G. and Kothe, A. (1997*), Steel Research*, 68, 266.

(10) Laird, L. and Smith, G. C. (1962), *Phil. Mag.*, 8, 847.

(11) Liaw, K., Swaminathnan, V.P and Leax, K. R. (1982), *Scri. Meta.*, 16, 871.

(12) Manson, S.S, Smith,R.W and Hirschberg, M.H. (1963), NASA TN D-1574

(13) Madariaga, I, Gutiérrez, I.,Capdevila, C. (1999*), Scripta Materialia*, 41,3,229

(14) Marrow, Jo Dean (1964): *Fatigue and Microstructure*, ASTM STP 45,378

(15) Muralitharan,U. and Manson, S.S (1988) *J. Engg. Mater. Tech.* 110, 55

(16) Naylor,D.J. (1998), in: *Microalloying Steel*: Rodriguez-lbabe, J.M. et. al.Trans Tech Publication,83.

(17) Paris, P. C and Frdogan, F. (1963), *Trans. ASME, J. Basic Engg.* 85(4),528.

(18) Pelloux, R.M.N. (1969), *Tran. ASM*, 62, 281.

(19) Plumbridge, W. J. (1972), *J. Marer. Sci.*, 6, 175.

(20) Ritchie, R.O. (1977), *Metal Science*, 11, 368.

(21) Ritchie, R. O. (1999), *Int. J. Fracture*, 100,55.

(22) Sharma, V.S, Sunderaraman, M. and Padmanabhan, K.A (1998), *Mat. Sc. Tech.* 14,669

(23) Suresh, S. (1997), *Fatigue of Materials*. London: Cambridge.

(24) Tamura, I.., Sekine, H., Tanaka, T., Ouchi, C (1988), *Thermo-mechanical Processing of High Strength Low Alloy Steels*. London: Butterworth

(25) Terazava,T., Higashiyama,H. and sekino,S.(1972), *Towards Improved Ductility and Toughness*, Japan, Climax molybdenum Co

(26) Tomkins,B. (1968), *Phil. Mag*, 18,1041

(27) Topper, T.H, Yu. T. (1989), *J. Fatigue*,11(5),335.

(28) Wohler, A. (1967), Engg, Aug 23,160.